HHS Public Access

Author manuscript

J Med Chem. Author manuscript; available in PMC 2021 November 29.

Published in final edited form as:

J Med Chem. 2020 October 22; 63(20): 12060–12072. doi:10.1021/acs.jmedchem.0c01394.

Design, Synthesis and Characterization of Benzimidazole Derivatives as PET Imaging Ligands for Metabotropic Glutamate Receptor Subtype 2 (mGluR2)

Gengyang Yuan[†,#], **Xiying Qu**[†,#], **Baohui Zheng**[†], **Ramesh Neelamegam**[†], **Sepideh Afshar**[†], **Suhasini M. Iyengar**[‡], **Chuzhi Pan**[†], **Junfeng Wang**[†], **Hye Jin Kang**[||], **Mary Jo Ondrechen**[‡], **Pekka Poutiainen**[⊥], **Georges El Fakhri**[†], **Zhaoda Zhang**[§,*], **Anna-Liisa Brownell**[†,*]

[†]Gordon Center for Medical Imaging, Massachusetts General Hospital and Harvard Medical School, 3rd Avenue, Charlestown, MA 02129, USA

[‡]Department of Chemistry and Chemical Biology, Northeastern University, 360 Huntington Avenue, Boston, MA 02115, USA

[§]Athinoula A. Martinos Center for Biomedical Imaging, Massachusetts General Hospital and Harvard Medical School, 149 Thirteenth Street, Suite 2301 Charlestown, MA 02129, USA

[||]Department of Pharmacology, University of North Carolina Chapel Hill School of Medicine, Chapel Hill, NC 27514, USA

[⊥]Department of Clinical Physiology and Nuclear Medicine, Kuopio University Hospital, Kuopio, 70210, Finland

Abstract

Three benzimidazole derivatives (**13**-**15**) have been synthetized as potential PET imaging ligands for mGluR2 in the brain. Of these compounds, **13** exhibits potent binding affinity (IC_{50} = 7.6 ± 0.9 nM), PAM activity (EC_{50} = 51.2 nM), and excellent selectivity against other mGluR subtypes (> 100-fold). [^{11}C]**13** was synthesized via *O*-[^{11}C]methylation of its phenol precursor **25** with [^{11}C]methyl iodide. The achieved radiochemical yield was 20 ± 2% (n = 10, decay-corrected) based on [^{11}C]CO_2 with radiochemical purity > 98% and molar activity 98±30 GBq/μmol EOS. *Ex vivo* biodistribution studies revealed reversible accumulation of [^{11}C]**13** and hepatobiliary and urinary excretions. PET imaging studies in rats demonstrated that [^{11}C]**13** accumulated in the mGluR2-rich brain regions. Pre-administration of mGluR2-selective PAM, **17** reduced the brain uptake of [^{11}C]**13**, indicating a selective binding. However, pre-administration of **13** significantly enhanced [^{11}C]**13** uptake in the brain. Therefore, [^{11}C]**13** is both a potential PET imaging ligand for mGluR2 and a drug candidate for the treatment of CNS disorders.

[*]**Corresponding Authors:** A-L.B.: phone, 617-726-3709; abrownell@mgh.harvard.edu, ZZ.: phone, 617-643-4887; zzhang@nmr.mgh.harvard.edu.

[#]Author Contributions

G.Y. and X.Q. contributed equally. The manuscript was written through contributions of all authors. All authors have given approval to the final version of the manuscript.

ASSOCIATED CONTENT

Supporting Information

The detailed *in vitro* assays and molecular modeling work are described in the Supporting Information.

The authors declare no conflict interest.

Graphical Abstract

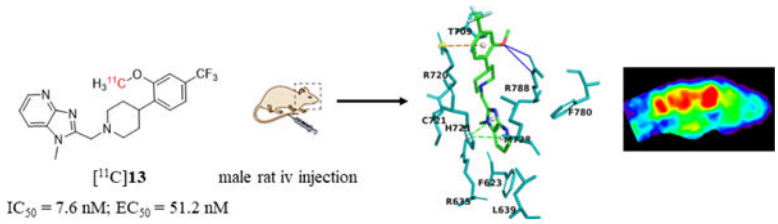

INTRODUCTION

The metabotropic glutamate receptor 2 (mGluR2) is widely expressed in the nervous systems.[1,2] mGluR2 expression is abundant in brain areas such as prefrontal cortex, hippocampus, amygdala, striatum, thalamus, cerebellum, and nucleus accumbens.[3,4] It predominantly localizes on presynaptic nerve terminals and modulates synaptic transmission and neuroplasticity.[3] Structurally, mGluR2 has a characteristic extracellular Venus flytrap domain (VFTD), a seven transmembrane (7-TM) domain and a cysteine rich domain (CRD) that connects the mGluR dimers.[5] The therapeutic benefits of mGluR2 modulators has been suggested for Alzheimer's disease[6–9], schizophrenia[10–13], depression[14], anxiety[15] and pain[16–18].

Initial research and drug discovery efforts had focused on pharmacological ligands for mGluR2/3, which have been published in literature and developed for the treatment of anxiety and schizophrenia in preclinical and clinical studies.[10–13,15] Until recently, mGluR2 and mGluR3 have been thought to have similar functions: they share high sequence homology, generally couple to Gi/o signaling, and provide negative feedback to reduce glutamate signaling. However, despite a successful phase 2 study conducted entirely in Russia for patients with schizophrenia, the clinical development of LY2140023, a mGluR2/3 receptor agonist prodrug, was halted due to lack of antipsychotic efficacy compared to placebo in three phase 2 or phase 3 trials.[12,19–21] The studies also revealed that the antipsychotic effect of mGluR2/3 agonists was absent in mGluR2 knockout mice but not mGluR3 knockout mice, suggesting the antipsychotic effects might be mediated via the mGluR2 but not mGluR3 receptor and even the effect of mGluR2 and mGluR3 might be different/opposite.[22,23]

Previously, we have reported two orthosteric antagonists as PET tracers, namely, [^{11}C]MMMHC (**1**) in 2003[24] and [^{11}C]CMGDE (**2**) in 2012[25], for Group II mGluRs (mGluR2 & mGluR3) (Figure 1). Since then, several PET radiotracers for mGluR2 have been derived from allosteric modulators that target the 7-TM instead of the VFTD region of mGluR2. It is believed that the allosteric modulators would bear higher lipophilicity and mGluR2 selectivity than orthosteric ligands due to the hydrophobicity and heterogeneity of the 7-TM binding pocket across mGlu receptors.[26–28] So far, two radioligands in this category have been advanced for human clinical trials, including mGluR2 PAM [^{11}C]JNJ42491293 (**3**) and a radioligand from Merck. However, [^{11}C]JNJ42491293 (**3**) was not found useful for the visualization and quantification of mGluR2 *in vivo* because of its apparent off-target binding.[29,30] The Merck radiotracer was only reported in an

abstract without information on its chemical structure and detailed imaging results.[31,32] The fluorine-18 labeled derivative of **3**, [^{18}F]FE-JNJ-42491293 (**4**), was disclosed in an abstract but it is not clear if this tracer has the similar off-target binding as **3**.[33] Recently, a mGluR2 PAM tracer [^{11}C]CMDC (**5**) and its three derivatives **6**-**8** were reported; however, **5** exhibited an insufficient affinity and low BBB-penetration. PET imaging with **5** did not enable *in vivo* visualization of the living rat brain.[34,35] On the other hand, three different types of mGluR2 NAM-based tracers were also disclosed. The mGluR2 NAM tracers [^{11}C]QCA (**9**)[36] and its analogue [^{11}C]**10**[37] showed off-target binding and limited brain uptake with intensive interaction with brain efflux pumps on the murine BBB. Two other types of NAM-based radiotracers have been disclosed in the patent literature. The compound **11** and its derivatives were patented as PET tracers for mGluR2/3.[38] The compound **12** and its derivatives were developed as mGluR2 PET ligands, but no *in vivo* PET imaging result has been described.[39]

The lack of efficient and efficacious mGluR2 PET tracers prompted us to further extend our previous effort toward exploration of mGluR2 PAMs as suitable PET imaging candidates. The benzimidazole derivatives have been the most widely examined series of mGluR2 PAMs in literature[27,40,41] with examples of highly potent mGluR2 ligands of compounds **13** (EC_{50} = 13 nM)[42] and **14** (EC_{50} = 5 nM, Figure 2)[41]. The presence of 2-methoxy-4-trifluoromethyl-phenyl group in compounds **13** and **14** allows rapid radiolabeling of their phenol precursors via *O*-[^{11}C]methylation with [^{11}C]CH_3I. We further designed compound **15** as a PET imaging candidate based on a potent mGluR2 PAM [2-(((1*R*,5*S*,6*r*)-6-((4-chloro-2-fluorophenoxy)methyl)-3-azabicyclo[3.1.0]hexan-3-yl)methyl)-1-methyl-1*H*-benzo[*d*]imidazole] (**16**, EC_{50} = 8 nM)[43] by replacing the distal 4-chloro-2-fluorophenoxy group with a 2-methoxy-4-(trifluoromethyl)phenoxy moiety. The structurally distinct compound **17**, a potent and selective mGluR2 PAM (EC_{50} = 78 nM),[44] was used as a selective blocking reagent during the investigation of [^{11}C]JNJ42491293 (**3**) and therefore we used it as a blocking reagent in the present studies.[30] Here, we report the design, synthesis and characterization of compounds **13**-**15** using *in silico* modeling, *in vitro* assays and *in vivo* PET imaging methods to evaluate their potential as mGluR2-selective PET imaging ligands.

RESULTS AND DISCUSSION

Chemistry.

Structurally, compounds **13**-**15** feature a merged heterocyclic core, a central cyclic amine core and a substituted distal arene. These compounds were synthesized according to reaction sequences delineated in Scheme 1. The intermediates **18**-**20** were prepared according to the reported procedures.[41,42] The intermediate **24** was synthesized in two steps: Mitsunobu reaction of **21** and **22**; followed by removal of N-Boc-group. Finally, compounds **13**-**15** were synthesized by the corresponding reductive amination reactions. Compound **17** was prepared according to the published procedure.[44]

Structural insights of compounds 13–15.

To provide structural insights on ligand-protein binding, compounds **13–15** were docked into a mGluR2 homology model, which was built in YASARA[45] (Supporting Information Figure S1 and Table S1) and validated by a series of structural analysis tools of ModFOLD[46], ERRAT and VERIFY 3D[47–49] (see Supporting Information Figures S2-S7). The key binding residues were predicted by Partial Order Optimum Likelihood (POOL)[50], DEPTH[51] and MetaPocket[52] (Supporting Information Figure S8). The docking experiments were performed at the 7-TM region with AutoDock embedded in YASARA (Supporting Information Table S2).[53] As shown in Figure 3, compounds **13–15** localize similarly at the entrance of the 7-TM region with their heterocyclic cores projecting to the bottom hydrophobic pocket and the distal substituted arenes interacting with residues at the extracellular loop 2 (EL2). Compound **13** has the best docking score of 8.7 kcal/mol compared to the values of 8.6 kcal/mol and 7.3 kcal/mol for compounds **14** and **15**, respectively. Compound **13** shows a hydrogen bonding interaction with Arg788, a π-cation interaction with Arg720, and a π- π stacking interaction with His723 (Figure 3). His723 has been previously reported as a key hydrophobic residue that interacts with several mGluR2 PAMs.[54,55] Compound **14** has similar key binding interactions as that of compound **13**, whereas, compound **15** exhibited fewer contacts in the binding pocket than compounds **13** and **14**, consistent with the decreased docking score. Overall, the *in silico* simulations suggest compounds **13-15** as potent mGluR2 binding ligands.

In vitro pharmacochemical properties.

To evaluate compounds **13-15**, the pharmacochemical properties including affinity to mGluR2, mGluR2 PAM activity, selectivity toward other mGluRs, lipophilicity, plasma protein binding, metabolic and solution stabilities as well as blood brain barrier (BBB) penetration capability were determined. In these studies, compound **13** was compared to the other two mGluR2 ligands **14** and **15**.

The binding affinity of compounds **13-15** was measured by the competitive binding assay in mGluR2 transfected CHO cells at the presence of 10 nM tritium-labeled radioligand [^{3}H]JNJ-46281222 (see Supporting Information).[56–58] The concentration of compounds **13-15** was increased from 0.01 nM to 10 μM to generate a competitive binding curve, with which the IC_{50} values were determined. As displayed in Table 1, compound **13** has potent binding toward mGluR2 (IC_{50} = 7.6 ± 0.9 nM), which is slightly stronger than those of compounds **14** (IC_{50} = 10.5 ± 0.5 nM) and **15** (IC_{50} = 10.5 ± 7.9 nM). The results also indicated that compounds **13-15** shared the same allosteric binding site of mGluR2.

Previously reported EC_{50} values for compounds **13** and **14** (EC_{50} = 13 nM and 5 nM, respectively)[36, 37] were determined by forced-coupling of mGluR2 to $G\alpha_{15}$ or $G\alpha_{16}$ followed by fluorescence detection of calcium flux upon activation. However, this assay is sub-optimal as it does not signal through the biorelevant cAMP pathway. Here, the mGluR2 PAM activity of compounds **13–15** was determined using Promega's split luciferase based GloSensor cAMP biosensor assay,[59,60] where, with this live cell assay, the mGluR2 PAM activity was evaluated in the presence of EC_{20} amount of L-glutamate by measuring changes in intracellular cAMP concentration, the relevant second

messenger mechanism. An mGluR2 PAM, [3'-(((2-cyclopentyl-6,7-dimethyl-1-oxo-2,3-dihydro-1*H*-inden-5-yl)oxy)methyl)-[1,1'-biphenyl]-4-carboxylic acid] (BINA),[61] was used as the reference compound for the assay. Figure 4 shows, the EC_{50} values of **13**, **14** and **15** are 51.2 nM, 101 nM and 7.8 μM, respectively, suggesting that **13** is a very potent mGluR2 PAM. The selectivity of **13–15** was also analyzed among the various mGluR subtypes, in which the G_q coupled receptors (mGluR1 and mGluR5) were tested using Ca^{2+} mobilization assay and the $G_{i/o}$ coupled receptors (mGluR2, mGluR3, mGluR4, mGluR6 and mGluR8) using cAMP assay. Results demonstrate that **13** has good selectivity against other mGlu receptors (> 100-fold, Supporting Information Table S3).

The physicochemical properties of compounds **13–15** were determined via ChemBiodraw (version 16.0) based on the molecular weight (MW), topological polar surface area (tPSA), and cLogP (Table 2). The experimental lipophilicity was measured by using liquid-liquid partition between *n*-octanol and water ("shake-flask method").[62] The LogP values obtained for compounds **13–15** were 3.65, 3.86 and 3.30 respectively, indicating their satisfactory CNS penetrating potentials (Supporting Information Table S5).[63] The plasma protein binding comprises compounds' binding to albumin, α1-acid glycoprotein and lipoproteins once delivered to the bloodstream. This property was evaluated for compounds **13** and **14** by equilibrium dialysis,[64] where two chambers were separated by a dialysis membrane (MWCO 8 kD). The plasma protein bindings of **13** and **14** are 87.2% and 88.7%, respectively (Supporting Information Tables 1 and S6). Therefore, the high plasma free fraction of compounds **13** and **14** (> 10%) would allow enough free drug concentration in blood stream to reach the brain targets.

The *in vitro* plasma and liver microsomal stability of **13** and **14** were studied by incubating the test compounds in rat serum and rat liver microsomes as well as NADPH cofactor, respectively, using previously published methods.[65,66] Diltiazem and ML128 (a mGluR4 PAM)[67,68] were used as co-assay QC controls for plasma and microsomal stability assays, respectively, to ensure that the assays were operating properly, and that the activity of the plasma and microsomes were consistent with established criteria. Compounds **13** and **14** are much more stable than diltiazem in rat plasma (Supporting Information Tables 3 and S7). The results also show that **13** and **14** exhibit reasonable microsomal stability and are much more stable than ML128, in which the suitable hepatic clearance of **13** and **14** is predicted (Supporting Information Tables 2 and S8-S9). The solution stability of **13** was evaluated with buffer solutions at pH 5.0, 7.4 and 9.4, respectively (Supporting Information Tables 3 and S10).[69] The results indicate that **13** is relatively stable in pH ranging from 5.0 to 9.4.

BBB penetration was a major barrier for some recently reported mGluR2 PET tracers that otherwise could have efficacy for imaging the brain target as shown by radiotracers [^{11}C]**9** and [^{11}C]**10**.[36,37] We have studied BBB penetration potential of compounds **13–15** with two *in vitro* assays, namely, parallel artificial membrane permeability assay (PAMPA) and Pgp-Glo™ assay. The PAMPA assay was carried out to predict passive BBB permeability.[70] Quality control standards were run with each sample set to monitor the consistency of the analysis. Verapamil was used as a high permeability standard ($P_e = 16 \times 10^{-6}$ cm/s) and theophylline was used as a low permeability standard ($P_e = 0.12 \times 10^{-6}$ cm/s). As Figure

5a shows, compound **13** has the best membrane permeability with an average effective permeability (P_e) value of 9.3×10^{-6} cm/s.

The Pgp-Glo™ assay was carried out on recombinant human P-gp in a cell membrane fraction to investigate whether the brain penetration will be affected by P-glycoprotein (P-gp) efflux transporter.[71] The effect of compounds **13–15** on P-gp ATPase activity was examined by comparing the untreated samples and the samples treated with **13–15** to sodium orthovanadate (Na_3VO_4)-treated control. The difference in luminescent signal between Na_3VO_4-treated samples and samples treated with the test compounds implied P-gp ATPase activity in the presence of the test compound. Verapamil, a P-gp substrate, was used as a positive control in the assay. By comparing basal and verapamil activities to that of **13–15**, it is clearly indicated that **13** is not a P-gp substrate and **15** is a potential P-gp substrate, while **13** displays a moderate P-gp ATPase activity (Figure 5b).

The *in vitro* pharmacological studies reveal that compound **13** has many CNS drug-like properties, including the potent mGluR2 PAM activity and good selectivity against other mGluRs, suitable lipophilicity and PPB, adequate metabolic stability, favorable passive permeability as measured by PAMPA, and no P-gp liability. Based on these results, compound **13** was selected for the radiolabeling and for *in vivo* evaluation as potential mGluR2 PET radioligand.

Radiochemistry.

The radiosynthesis of [^{11}C]**13** was achieved via the one-step *O*-methylation of its phenol precursor **23**. Compound **23** was synthesized by demethylation of **13** using boron tribromide (Scheme 2). The radiosynthesis of [^{11}C]**13** was performed by the reaction of **23** (0.5 ± 0.1 mg) with [^{11}C]CH_3I in the presence of aqueous NaOH (5N, 3 μL) in dry DMF (250 μL). The reaction was carried out at 80 °C for 2 min, followed by purification using a semi-preparative HPLC (Figure S9). The identity of [^{11}C]**13** was confirmed by co-injection with the unlabeled **13** on an analytical HPLC (Figure S10). The radiochemical yield was 20 ± 2% decay-corrected (n = 10), calculated from starting [^{11}C]CO_2. The [^{11}C]**13** was then formulated into 10% ethanolic saline solution (pH = 5–6) before injection. The radiochemical and chemical purity were greater than 98%, and the molar activity was 98 ± 30 GBq/μmol at the end of synthesis (EOS). The overall synthesis time was ca. 50 min, and no radiolysis was observed up to 90 min.

Ex vivo biodistribution studies.

The *ex vivo* whole body biodistribution of [^{11}C]**13** was performed in 16 normal male Sprague Dawley rats after intravenous injection of [^{11}C]**13** at several time points (5, 20, 30 and 40 min). The uptake value is expressed in the unit of % ID/g. These studies support reversible accumulation of [^{11}C]**13** with the highest accumulation 5 min after administration of radioactivity in other investigated tissue areas but the lungs where the maximum accumulation was at 20 min and the muscle where the radioactivity steadily increased up to 40 min (Figure 6). The highest accumulation was measured in the liver (2.73 ± 0.02% ID/g) followed by kidney (1.05 ± 0.07% ID/g), spleen (0.67 ± 0.05% ID/g), lung (0.59 ± 0.04% ID/g), and heart (0.58 ± 0.05% ID/g). The high radioactivity uptake in liver

and kidney suggest that hepatobiliary elimination and renal excretion contribute to the whole body distribution of [^{11}C]**13**. The average accumulation of [^{11}C]**13** in the rat brain at 5 min was 0.49 ± 0.07% ID/g. This result indicates a rapid BBB penetration of [^{11}C]**13**, which was consistent with the following *in vivo* brain imaging studies.

PET imaging.

In vivo characterization of [^{11}C]**13** was conducted with PET imaging using rat (male Sprague-Dawley) models. Dynamic PET scans were performed for 60 min after tail vein injection of [^{11}C]**13**. Representative PET images of cumulative volumetric distribution of [^{11}C]**13** at time interval of 10–15 min are shown on five coronal, axial and sagittal levels (Figure 7). The accumulation of [^{11}C]**13** clearly delineates the mGluR2-rich regions in the rat brain. Time-activity curves (TACs) showed fast radioactivity uptake (SUV_{max} = 1.8 ± 0.2, n = 9) and time-dependent accumulation of radioactivity in different brain regions. The highest accumulation of [^{11}C]**13** was in the thalamus, followed by striatum, cerebellum, and cortex. (Figure 8a). Blocking studies were conducted to investigate mGluR2-selective binding of [^{11}C]**13**. Pretreatment with the structurally distinct *in vivo* active mGluR2 PAM ligand **17** (4 mg/kg i.v.) 10 min before [^{11}C]**13** injection resulted in a 28–37% decrease of [^{11}C]**13** uptake in different brain areas at the 10–30 min time window (Figure 8b). On the other hand, administration of unlabeled compound **13**, using a dose of 4 mg/kg iv. 10 min before [^{11}C]**13** injection, resulted in a 33–49% enhancement of radioactivity uptake in the different brain areas at the same time window as mentioned above. These results confirm that [^{11}C]**13** has *in vivo* mGluR2-selective binding in the rat brain. The significant increase of radioactivity uptake after self-blocking indicates that the compound **13**, as a mGluR2 PAM, is capable of potentiating strong pharmacological effects, making **13** a potential candidate for therapeutic approaches.

CONCLUSION

We have synthesized and characterized three benzimidazole derivatives (**13–15**) as mGluR2 PAMs. Compound **13** demonstrated nanomolar binding potency toward mGluR2 and excellent selectivity over other mGluRs. Further *in vitro* pharmacological and brain permeability evaluations confirmed the potential of compound **13** as PET imaging ligand. A robust and reliable one-step radiosynthetic procedure was established for radiolabeling compound **13** with carbon-11. The desired product [^{11}C]**13** was obtained with a radiochemical yield of 20 ± 2 % (n = 10, decay-corrected) based on [^{11}C]CO_2 and a molar activity of 98 ± 30 GBq/μmol at the end of synthesis (50 min). The *ex vivo* pharmacokinetic results of [^{11}C]**13** suggested its reversible accumulation in most tissue areas and hepatobiliary & urinary excretions. PET imaging studies indicated that [^{11}C]**13** crossed the BBB rapidly and was mainly accumulated in the mGluR2-rich regions of the rat brain such as the thalamus, cerebellum, striatum and cortex. The blocking studies using mGluR2-selective PAM (**17**) significantly reduced the [^{11}C]**13** uptake in these brain regions, indicating the highly selective uptake of [^{11}C]**13** in rat brain. Distinct from previous observations of mGluR2 PET radioligands, self-blocking of [^{11}C]**13** resulted in an apparent uptake increase in the accumulation by almost 50%. This result indicates a significant

modulation effect of compound **13** *in vivo* as mGluR2 PAM, which bears promising therapeutic applications for translational studies in neurological conditions and/or disorders.

Altogether, these results suggest that compound **13** might have two different application areas. When radiolabeled with carbon-11 it will be a potential PET imaging ligand for mGluR2 in the brain and when used as a drug (cold compound) it might be a therapeutic drug for different neurological conditions and diseases which are affected by mGluR2 malfunction.

EXPERIMNETAL SECTION

Animal Procedures.

The animal studies were approved and done under the guidelines of the Subcommittee on Research Animals of the Massachusetts General Hospital and Harvard Medical School in accordance with the Guide of NIH for the Care and Use of Laboratory Animals.

Materials and Methods.

All reagents and starting materials were obtained from the commercial sources including Sigma-Aldrich (St. Louis, MO), Thermo Fisher Scientific, Oakwood Products, Inc., Matrix Scientific, Acros Organics and used as received. The reactions were monitored by TLC using a UV lamp monitored at 254 nm. If necessary, the reactions were also checked by LC−MS using the Agilent 1200 series HPLC system coupled with a multi-wavelength UV detector and a model 6310 ion trap mass spectrometer (Santa Clara, CA) equipped with an Agilent Eclipse C8 analytical column (150 mm × 4.6 mm, 5 μm). Elution was with a 0.1% formic acid solution of water (A) and acetonitrile (B). The silica gel used in flash column chromatography was from Aldrich (Cat. 60737, pore size 60 Å, 230–400 mesh). Flash chromatography was also performed with a CombiFlash Rf Purification System (Teledyne Isco) using a Silica ReadySep Rf column. The products were identified by LC−MS as well as ^{1}H NMR, ^{13}C NMR and ^{19}F NMR using a Varian 500 MHz spectrometer. All NMR samples were dissolved in chloroform-d ($CDCl_3$), methanol-d_4 (CD_3OD) or DMSO-d_6 [$(CD_3)_2SO$] containing tetramethylsilane as a reference standard. Chemical shifts were expressed as ppm and calculated downfield or upfield from the NMR signal of reference standard. *J* was expressed as Hz, and its splitting patterns were reported as s, d, t, q, or m. HRMS was obtained from the High-Resolution Mass Spectrometry Facility at the University California, Riverside, using electrospray ionization (ESI)/atmospheric pressure chemical ionization (APCI) technique (Agilent Time of Flight (TOF) LC−MS). Unless otherwise specified, the purities of all new compounds were over 95% determined by HPLC.

Chemistry. tert-Butyl(1R,5S,6R)-6-((2-methoxy-4-(trifluoromethyl)phenoxy)methyl)-3-azabicyclo [3.1.0] hexane-3-carboxylate (23).

2-methoxy-4-(trifluoromethyl)phenol (**22**, 0.45 g, 2.3 mmol) and triphenyl phosphine (0.9 g, 3.5 mmol) were added to a solution of (*1R,5S,6R*)-tert-butyl 6-(hydroxymethyl)-3-azabicyclo[3.1.0]hexane-3-carboxylate (**21**, 0.5 g, 2.3 mmol) in THF under nitrogen. Diethyl azodicarboxylate solution (40 wt. % in toluene, 1.5 g, 3.5 mmol) was added and the reaction was stirred for 16 h. The reaction mixture was stripped in *vacuum* to give orange oil. The

crude product was purified via flash chromatography to give **23** as a white solid (0.44 g, 1.14 mmol, 48% yield). ^{1}H NMR (500 MHz, $CDCl_3$) δ ppm 7.18 (dd, J = 1.0, 8.5 Hz, 1H), 7.08 (d, J = 1.8 Hz, 1H), 6.89 (d, J = 8.4 Hz, 1H), 4.04–4.08 (m, 1H), 3.92 (s, 3H), 3.82–3.92 (m, 1H), 3.58–3.72 (m, 2H), 3.33–3.42 (m, 2H), 1.59 (d, J = 2.7 Hz, 2H), 1.45 (s, 9H), 1.18–1.25 (m, 1H). ^{13}C NMR (125 MHz, $CDCl_3$) δ ppm 154.8, 150.8, 149.5, 124.3 (q, J = 271.3 Hz), 123.3 (q, J = 32.7 Hz), 118.2 (q, J = 4.2 Hz), 112.7, 108.5 (q, J = 3.6 Hz), 79.4, 70.7, 56.1, 28.5, 21.4. LC-MS calculated for $C_{19}H_{24}F_3NO_4$: 387.17; observed: m/z 410.0 $[M+Na]^+$.

(1R,5S,6R)-6-((2-methoxy-4-(trifluoromethyl)phenoxy)methyl)-3-azabicyclo[3.1.0] hexane (24).

Trifluoroacetic acid (1 mL) was added to a solution of **23** (0.44 g, 1.14 mmol) in dichloromethane (5 mL). The mixture was stirred at room temperature for 2 h. The solvent was removed under reduced pressure to give **24** as a yellow oil (0.3 g, 1.05 mmol, 92% yield). ^{1}H NMR (300 MHz, methanol-d_4) δ ppm 7.16–7.24 (m, 2H), 7.05 (d, J = 8.3 Hz, 1H), 4.0 (d, J = 6.7 Hz, 2H), 3.88 (s, 3H), 3.42–3.53 (m, 4H), 1.94–1.98 (m, 2H), 1.39–1.47 (m, 1H). ^{13}C NMR (75 MHz, methanol-d_4) δ ppm 152.4, 151.1, 125.8 (q, J = 270.5 Hz), 124.4 (q, J = 32.6 Hz), 119.4 (q, J = 4.2 Hz), 114.4, 109.7 (q, J = 3.6 Hz), 70.7, 56.7, 22.2, 21.0. LC-MS calculated for $C_{14}H_{16}F_3NO_2$: 287.11; observed: m/z 288.1 $[M+H]^+$.

2-((4-(2-Methoxy-4-(trifluoromethyl)phenyl)piperidin-1-yl)methyl)-1-methyl-1H-imidazo[4,5-b]pyridine (13).

Trimethylamine (0.22 g, 2.16 mmol), magnesium sulfate (0.65 g, 5.41 mmol) and 1-methyl-1H-imidazo[4,5-b]pyridine-2-carbaldehyde (**19**, 0.81 mmol, 0.16 g) were added to a solution of 4-(2-methoxy-4-(trifluoromethyl)phenyl)piperidine (**18**, 0.54 mmol, 0.13 g) in 1,2-dichloroethane (5 mL) under nitrogen. The mixture was stirred at room temperature for 30 min before sodium triacetoxyborohydride (0.17 g, 0.81 mmol) was added. The reaction mixture was then stirred overnight at room temperature and then quenched with dichloromethane. The organic phase was washed with water and brine. The aqueous phase was extracted with dichloromethane. Combined organic layer was dried over sodium sulfate. The solvent was removed at reduced pressure, and the residue was purified by flash column chromatography to give the product as a white solid (0.35 mmol, 0.14 g, 65% yield). ^{1}H NMR (500 MHz, CD_3OD): δ 8.41 (d, J = 5.0 Hz, 1H), 8.02 (d, J = 8.5 Hz, 1H), 7.34–7.37 (m, 2H), 7.20 (d, J = 7.5 Hz, 1H), 7.14 (s, 1H), 4.01 (s, 3H), 3.94 (s, 2H), 3.89 (s, 3H), 3.31–3.32 (m, 3H), 2.33–2.37(m, 2H), 1.72–1.83 (m, 4H). LC-MS calculated for $C_{21}H_{23}F_3N_4O$: 404.18; observed: m/z 405.15 $[M+H]^+$.

2-((4-(2-Methoxy-4-(trifluoromethyl)phenyl)piperidin-1-yl)methyl)-5,6-dihydro-4H-imidazo [4,5,1-ij][1,7]naphthyridine (14).

In a similar procedure as described for synthesizing **13**, compound **14** was prepared by using **18** (100 mg, 0.34 mmol) and 5,6-Dihydro-4H-imidazo[4,5,1-ij][1,7]naphthyridine-2-carbaldehyde (**20**, 110 mg, 0.51 mmol) to give the product as a white solid (76 mg, 0.18 mmol, 52% yield). ^{1}H NMR (500 MHz, $(CD_3)_2SO$): δ 8.50 (d, J = 5.0 Hz, 1H), 7.40 (d, J = 8.5 Hz, 1H), 7.25 (d, J = 8.5 Hz, 1H), 7.20 (s, 1H), 7.01 (d, J = 4.5 Hz, 1H,), 4.33 (t, J = 6.0 Hz, 2H), 4.02 (s, 1H), 3.29 (s, 1H), 3.86 (s, 3H), 2.93–2.97 (m, 5H), 2.15–2.48

(m, 5H), 1.60–1.71 (m, 4H). LC-MS calculated for $C_{23}H_{25}F_3N_4O$: 430.20; observed: *m/z* 431.20 $[M+H]^+$.

2-(((1R,5S,6R)-6-((2-methoxy-4-(trifluoromethyl)phenoxy)methyl)-3-azabicyclo[3.1.0]hexan-3-yl)methyl)-1-methyl-1H-imidazo[4,5-b]pyridine (15).

In a similar procedure as described for synthesizing **13**, compound **15** was prepared by using **19** (HCl salt, 50 mg, 0.25 mmol) and **24** (HCl salt, 98 mg, 0.304 mmol) to give product as a white solid (31 mg, 0.072 mmol, 28% yield). ^{1}H NMR (500 MHz, $CDCl_3$): *δ* 8.47 (d, *J* = 4.5 Hz, 1H), 7.59 (d, *J* = 7.5 Hz, 1H), 7.29 (m, 2H), 7.02 (s, 1H), 6.83 (d, *J* = 8.5 Hz, 1H), 3.93 (s, 2H), 3.85 (s, 3H), 3.83 (d, *J* = 7.5 Hz, 2H), 3.78 (s, 3H), 2.96 (d, *J* = 9.0 Hz, 2H), 2.57 (d, *J* = 8.0 Hz, 2H), 1.67(m, 1H), 1.50 (s, 2H). ^{13}C NMR (125 MHz, $CDCl_3$): *δ* 155.0, 154.4, 151.0, 149.3, 144.5, 128.4, 123.1, 122.8, 118.2, 117.6, 116.9, 112.4, 108.4, 71.3, 56.0, 54.5, 51.5, 30.1, 21.5, 18.6. ^{19}F NMR (470 MHz, $CDCl_3$): δ −57.6. LC-MS calculated for $C_{22}H_{23}F_3N_4O_2$: 432.18; observed: *m/z* 433.15 $[M+H]^+$. HRMS m/z calculated for $C_{22}H_{24}F_3N_4O_2$ $[M+H]^+$, 433.1851, found *m/z* 433.1863.

3-(Cyclopropylmethyl)-7-((4-(2,4-difluorophenyl)piperazin-1-yl)methyl)-8-(trifluoromethyl)[1,2,4]triazolo[4,3-a]pyridine (17, JNJ-46356479).

In a similar procedure as described for synthesizing **13**, compound **17** was prepared by using 3-(cyclopropylmethyl)-8-(trifluoromethyl)-[1,2,4]triazolo[4,3-a]pyridine-7-carbaldehyde (50 mg, 0.19 mmol) and 1-(2,4-difluorophenyl)piperazine (41.6 mg, 0.21 mmol), TEA (0.11 mL, 0.76 mmol), $MgSO_4$ (0.229 g, 1.9 mmol) and $NaBH(OAc)_3$ (60.4 mg, 0.285 mmol) in DCM (3 mL) to give product as a pale-yellow solid (44.2 mg, 0.098 mmol, 51.6% yield). ^{1}H NMR (500 MHz, $CDCl_3$) *δ* 8.23 (d, *J* = 7.5 Hz, 1H), 7.45 (d, *J* = 6.5 Hz, 1H), 6.90−6.91 (m, 1H), 6.78–6.81 (m, 2H), 3.81 (s, 2H), 3.10 (d, J = 6.5 Hz, 2H), 3.01–3.09 (m, 4H), 2.63–2.75 (m, 4H), 1.21–1.26 (m, 1H), 0.60–0.62 (m, 2H), 0.33–0.34 (m, 2H). LC-MS calculated for $C_{22}H_{22}F_5N_5$: 451.18; observed: *m/z* 452.05 $[M+H]^+$.

2-(1-((1-Methyl-1H-imidazo[4,5-b]pyridin-2-yl)methyl)piperidin-4-yl)-5-(trifluoromethyl)phenol (25).

The boron tribromide solution (1 mL, 1 M in DCM, 1 mmol) was added dropwise to a solution of compound **13** (70 mg, 0.173 mmol) in 3 mL dichloromethane at 0 ℃. The mixture was slowly warmed to room temperature and stirred for another 2 h. After the reaction was completed, 5 mL of saturated sodium bicarbonate was added, and the mixture was extracted with dichloromethane. The crude product was purified by flash column chromatography to give product as a white solid (60 mg, 0.153 mmol, 88% yield). ^{1}H NMR (500 MHz, CD_3OD): *δ* 8.42 (d, *J* = 5.0 Hz, 1H), 8.03 (d, *J* = 8.5 Hz, 1H), 7.34–7.37 (m, 1H), 7.28 (d, *J* = 7.5 Hz, 1H), 7.05 (d, 1H, *J* = 7.5 Hz), 7.00 (s, 1H), 4.01 (m, 3H), 3.94, (m, 2H), 2.99–3.06 (m, 3H), 2.34–2.38 (m, 2H), 1.73–1.86 (m, 4H). ^{13}C NMR (125 MHz, CD_3OD): *δ* 155.4, 155.0, 153.7, 143.6, 136.6, 128.7, 126.8, 125.4, 123.3, 118.7, 118.0, 115.3, 115.3, 111.0, 54.6, 54.2, 35.1, 31.3, 29.5. LC-MS calculated for $C_{20}H_{21}F_3N_4O$: 390.17; observed: *m/z* 391.10 $[M+H]^+$. HRMS *m/z* calculated for $C_{20}H_{22}F_3N_4O$ $[M+H]^+$, 391.1746, found *m/z* 391.1765.

Radiochemistry.

$^{11}CO_2$ was obtained via the $^{14}N(p,\alpha)^{11}C$ reaction on nitrogen with 2.5% oxygen, 16 MeV protons (GE Healthcare, PETtrace), and trapped on molecular sieves in a TRACERlab FX-MeI synthesizer (GE Healthcare). $^{11}CH_4$ was obtained by the reduction of $^{11}CO_2$ in the presence of hydrogen at 350 °C and passed through an oven containing I_2 to produce $^{11}CH_3I$ via a radical reaction. $^{11}CH_3I$ was trapped in a 5 mL V-vial containing a solution of excess **25** (0.5 ± 0.2 mg) and an aqueous 5N NaOH (3 uL) in dry dimethylformamide (250 μL) at room temperature and then heated at 80 °C for 2 min. The reaction mixture was diluted with 1.0 mL of water and purified using a HPLC system equipped with a semi-preparative column (Waters XBridge, C18, 250 × 10 mm, 5 μ), a UV detector monitored at 254 nm, and a radioactivity detector. The product was eluted with acetonitrile/water/TFA (30/70/0.7) at a flow rate of 5 mL/min. The fractions corresponding to [^{11}C]**13** (t_R = 11 min) were collected into a large dilution vessel, which was pre-loaded with 2 mL of 8.4% sodium bicarbonate for injection, USP (Hospira) and 23 mL of sterile water for injection, USP. The product was loaded onto a C18 light cartridge, (Waters; pre-activated with 4 mL of EtOH followed by 10 mL of SWFI). The C18 light cartridge was washed with 10 mL of SWFI to remove traces of salts, residual acetonitrile and TFA. The C18 light cartridge was then eluted with 1 mL of dehydrated ethyl alcohol (USP) and followed by 10 mL of 0.9% sodium chloride solution (USP) into a product collection vessel. The formulated solution was filtered through a vented Millipore-GV 0.22μ sterilizing filter (EMD Millipore) into a 10 mL vented sterile vial.

Radiochemical purity and chemical quality were measured by an analytical HPLC equipped with an analytical column (Waters, XBridge, C18, 3.5 μ, 4.6 × 150 mm), a UV detector monitored at 254 nm, and a radioactivity detector, which was eluted with a solution (acetonitrile/0.1%TFA water = 30/70) at a flow rate of 1 mL/min. [^{11}C]**13** was eluted ~6 min (chemical and radiochemical purities > 98%, n = 10). The radiosynthesis time was 50 min from the end of bombardment (EOB). The molar activity was 98 ± 30 GBq/μmol at the end of synthesis (EOS).

Molecular modeling.

The mGluR2 receptor model structure was built in YASARA[45] using a series of structures from the Protein Data Bank (PDB). These structures were obtained after a BLAST[72] search of the mGluR2 sequence against the PDB. The model was built by manually selecting from these template structures with sequence homology to mGluR2. These templates are mGluR1 complexed with glutamate (PDB ID:1EWK)[73], mGluR5 complexed with glutamate (PDB ID: 3LMK)[74] and Metabotropic Glutamate Receptor 5 Apo Form (PDB ID 6N52)[75]. Using these three structures as templates, a hybrid model for mGluR2 was built in YASARA. Results of model evaluations are given in the Supporting Information.

To prepare the ligands for docking, the ligands were drawn on ChemDraw Professional 16.0 by PerkinElmer and were converted into PDB format in Avogadro 1.2[76]. These ligands were further optimized in Avogadro before docking. Docking was performed into the model structure with AutoDock[53] embedded in YASARA[45].

GloSensor cAMP functional assay.

HEK-293 cells were maintained with complete Dulbecco's modified Eagle's medium (DMEM), which was composed of 10% fetal bovine serum (FBS), 2 mM L-glutamine, 100 units/mL penicillin G, 100 μg/mL streptomycin at 37 °C in the presence of 5% CO_2. HEK-293 stable cell lines with tetracycline inducible expression of mGluR1, mGluR2, mGluR4, mGluR6 or mGluR8 were maintained with complete DMEM with Hygromycin B (100 μg/mL), Blasticidin (15 μg/mL) at 37°C in the presence of 5% CO_2.

The Gq coupled receptors (mGluR1 and mGluR5) were tested using Ca^{2+} mobilization assay. mGluR1 stable cell lines were plated into poly-L-lysine (PLL) coated 384-well black clear bottom cell culture plates with complete Basal Medium Eagle (BME) buffer, which was composed of 10% dialyzed FBS, penicillin G (100 units/mL), streptomycin (100 μg/mL) with Tetracycline (1 μg/mL) at density of 20,000 cells in 40 μl per well for overnight. On the other hand, HEK-293 Cells transiently transfected using the calcium phosphate method with cDNA encoding mGluR5 for 40 h were plated into the plate with complete BME at density of 20,000 cells in 40 μL per well for 8 h. mGluR1 stable cells or cells transiently expressing mGluR5 were incubated with 20 μL of the calcium dye (FLIPR Calcium 4 Assay Kit; Molecular Devices) diluted in the assay buffer (1× HBSS, 2.5 mM probenecid, and 20 mM HEPES, pH 7.4) for 45 min at 37 °C and 15 min at room temperature. To measure agonist activity of receptors, the drug plates were prepared with different concentrations of test or reference compound at 3 times the desired final concentration. When measuring antagonist activity, another drug plate which contained EC_{80} concentration of the reference drug was prepared. Once loaded in FLIPR (Molecular Devices), basal fluorescence was measured for 10 s, then 10 μL of test or reference compounds were added, followed by continued fluorescence measurement for an additional 120 s. Raw data were plotted as a function of molar concentration of the compound with Prism 5.0 (GraphPad Software).

The Gi/o coupled receptors (mGluR2, mGluR3, mGluR4, mGluR6 and mGluR8) were tested using cAMP assay. Promega's split luciferase based GloSensor cAMP biosensor technology was used in determining Gi-GPCR mediated cAMP production in live cells. On the cells stably expressing mGluR2, mGluR3, mGluR4, mGluR6 or mGluR8, GloSensor cAMP DNA construct was transfected overnight. Cells were seeded into PLL coated 384-well white clear bottom cell culture plates with complete BME Buffer with Tetracycline (1 μg/mL) at a density of 20,000 cells for another 24 h. The cell medium was removed and then 20 μl of buffer was loaded. To measure the agonist activity, 10 μL of 3x test compound solution was added 15 min before addition of 10 μl of luciferin/isoproterenol mixture at a final concentration of 4 mM and 200 nM, respectively, followed by counting of the plate. To measure the PAM or antagonist activity, cells were pre-incubated with test compound for 15 min before addition of EC_{20} or EC_{80} concentration of a reference agonist for another 15 min. Then 10 μl of luciferin/isoproterenol mixture at a final concentration of 4 mM and 200 nM, respectively, was added for 15 min followed by counting of the plate. In these experiments, isoproterenol was used to activate endogenous β_2 adrenergic receptors expressed in HEK293 T cells to activate the endogenous G_s protein. Luminescence was

counted in a TriLux luminescence counter. Data were analyzed with Prism 5.0 (GraphPad software).

Compounds were tested for their potency in dose-response experiments. Eight-point dose response curves were performed in duplicate twice on two separate lots of cells (sometimes a third curve might be needed if in the first experiment the range of concentrations used was outside of the active range). For antagonists, these curves were performed in the presence of the EC_{80} concentration of the agonist. For each compound, the results from four replicates were averaged and then either EC_{50} or IC_{50} values were calculated by non-linear regression using the 4-parameter logistic equation. Results were reported as EC_{50} or IC_{50} values for each tested compound (and receptor) and include the EC_{50} or IC_{50} values of a known agonist or antagonist for comparison purposes.

In vitro characterization.

The Log P was determined using a reversed-phase HPLC method. First, seven reference compounds were examined to obtain the linear regression of the log P against the log of capacity factors by the expression: $\log P_{ow} = a + b * \log k$. The Log P of these reference compounds was already been determined. The capacity factor k was calculated by the expression: $k = (t_R - t_0)/t_0$. The retention time t_R of test compound was determined on the HPLC (Agilent 1260 infinity II LC System, XTerraTM MS C18 5μ 2.1 × 250 mm, methanol/water=75/25, 0.25 mL/min). The dead-time t_0 was measured by using thiourea. All measurements were done with triplicate three parallels and results are given in Table S4. The linear regression equation of the Log P against the log of capacity factors was generated in Excel: $\log P_{ow} = 3.049 + 2.429 * \log k$, where R^2 was 0.9964 (Figure S9). The retention time of compound **13–15** was also determined on the HPLC under the same condition and each test was repeated three times (Table S5).

In the plasma protein binding assay, disposable RED device inserts (product 90006) were from Thermos Scientific (Waltham, MA). Each insert was made of two side-by-side chambers separated by a vertical cylinder of dialysis membrane (MWCO ~8,000) validated for minimal non-specific binding. A stock solution of the test compound in DMSO was spiked into the rat plasma to reach a concentration of 10 μM. 400 μL of sample solution was placed into the sample chamber of the RED device, and 600 μL of phosphate-buffered saline (PBS) was added to the buffer chamber of the RED device. Samples were prepared in triplicates. The plate was covered with aluminum sealing cover and incubated at 37 °C on an orbital shaker at approximately 200 rpm for 5 h. After incubation, 300 μL of post-dialysis samples from the buffer and sample chambers were transferred to different microcentrifuge tubes. To the buffer sample was added 300 μL of plasma, and an equal volume of buffer was added to the collected plasma sample. 600 μL of cold acetonitrile was added to the samples, and the samples were vortexed and incubated for 30 min on ice and then were centrifuged at 14000 rpm for 10 min. Supernatant was transferred to vial for HPLC analysis (XTerraTM MS C18 5μ, 2.1 × 250 mm column; Gradient elution from 5% to 90% B in 30 min; 0.1 M ammonium formate in water (A) and acetonitrile (B); UV 254 nm; 100 uL of injection volume). The percentage of the test bound compound was calculated as % Free

= (Concentration in buffer chamber/Concentration in plasma chamber) ×100%; % Bound = 100% - % Free (Table S6).

Compound stability in rat serum was examined using a published method.[65] Rat serum (100 μL, Abcam, Inc, No. ab7488) and test compound or control compound (2.5 μL, 1 mM in DMSO) was added to the individual tube. The tube was vortexed and incubated at 37 °C. During the incubation, aliquots of 50 uL samples were quenched with ice-cold acetonitrile at 0, 15, 30, 60, and 120 min time points, respectively. After mixing, the quenched samples were centrifuged, and the supernatant was withdrawn for analysis by HPLC (Agilent 1260 infinity II LC System, XTerraTM MS C18, 5 μ, 2.1 × 250 mm, 20 mM ammonium formate (A)/acetonitrile (B), 0.25 mL/min, gradient of 5% to 100% B). The samples were assayed at least three times. Compound **25** was used as internal standard while diltiazem was used as a positive control. The percentage remaining was calculated by (peak area at the specific time point)/(peak area at 0 min) × 100% (Table S7).

Compound stability in rat liver microsomal was tested using a published method.[65,66] In a vial 1.5 μL of test compound (1 mM in DMSO stock solution) was mixed with 432 μL of PBS (50 mM, pH 7.4). The mixture was kept at 37 °C for 10 min before adding 13 μL of Sprague−Dawley rat liver microsomes (Sigma-Aldrich, No. M9066). The vial was vortexed and shaken at 37 °C for 5 min, followed by addition of 50 μL of NADPH (10 mM in PBS stock solution) to start the reaction. The mixture was incubated at 37 °C for 0, 5, 15, 30, 45 min, respectively, and quenched by addition of 250 μL of ice-cold acetonitrile and 3 μL of the internal standard (0.5 mM in DMSO). The quenched solutions were centrifuged at 10,000g for 15 min. The supernatant was collected and quantitated by RP-HPLC (Phenomenex Luna® column 5 μ C18, 100 Å, 250 × 4.6 mm; 0.7 mL/min, 15 min, Acetonitrile/water/0.1% FA). The procedure was repeated three times for each compound. Compound **25** was used as internal standard and compound ML128 served as positive control. The percentage of remaining intact test-compound was calculated by (peak area at the specific time point)/(peak area at 0 min)×100%. Each procedure was repeated three times (Tables S8 & S9).

The solution stability of **13** was examined in the aqueous buffers at different pH values. 50 μL of compound in DMSO (0.25 mM) was added to the sodium acetate-KCl-HCl buffer (950 μL, 20 mM, pH 5.0), phosphate buffer (950 μL, 20 mM, pH 7.4), and boric acid-KCl-NaOH buffer (950 μL, 20 mM, pH 9.4), respectively. The mixtures were incubated for 2 h at 37 °C and analyzed by HPLC (Phenomenex Luna® column, 5 μm C18, 100 Å, 250 × 4.6 mm, eluents: CH_3CN/H_2O in 0.1% formic acid). The area under curve (AUC) values of **13** was monitored at 0, 15, 30, 60, and 120 min time points (n = 2, Table S10).

In the PAMPA assay, polar brain lipid (PBL) was purchased from Avanti Polar Lipids (Alabaster, AL). Theophylline, caffeine, and dodecane were purchased from Sigma-Aldrich. The 96-well acceptor filter plate (polyvinylidene difluoride membrane, pore size 0.45 μm) and the donor microplate were obtained from Merck Millipore Bioscience (Bedford, MA). Test compound was dissolved in DMSO at 5 mg/mL, and further diluted in phosphate buffer (pH 7.4) to obtain the sample solution at a final concentration of 25 μg/mL. The acceptor wells were coated with 4 μL of porcine polar brain lipid (PBL) in dodecane (20 mg/mL)

before 200 μL of phosphate buffer was added. To the corresponding donor well, 300 μL of the sample solution (n = 5) was added. The acceptor well was carefully put on the donor plate and kept for 18 h. After incubation, the acceptor plate was separated from the donor plate and the concentration of the test compounds in both acceptor and donor wells was determined using a UV plate reader (SpectraMax M Series Multi-Mode Microplate Readers). Verapamil (P_e = 16 ×10^{-6} cm/s) and theophylline (P_e = 0.12 ×10^{-6} cm/s) were used as positive and negative control compounds, respectively.

The P-gp ATPase activity was measured with the Pgp-Glo™ assay system with human P-gp membrane by following the manufacturer's instructions (Promega, Co. USA). The assay relies on the ATP dependence of the light-generating reaction of firefly luciferase. Briefly, 25 μg of P-gp membrane was incubated at 37 °C with one of these samples including Na_3VO_4 (100 μM), solvent control (0.1% DMSO), quercetin (100 μM), the test compound (200 μM), verapamil (100 μM), verapamil (100 μM) plus the test compound (100 μM). The ATPase reaction was initiated by addition of MgATP (5 mM) and followed by incubation for 40 min at 37 °C. The reaction was stopped, and the remaining unmetabolized ATP was detected as a luciferase-generated luminescence signal by addition of ATP detection reagent. Following a room-temperature signal-stabilization period (20 min), luminescence was read on a Veritas microplate luminometer (Tuner Designs, San Francisco, CA). P-gp ATPase activity was presented as a drop-in luminescence of samples compared to that treated with Na_3VO_4.

Whole body biodistribution study.

The quantitative biodistribution of [^{11}C]**13** was done using 16 healthy Sprague Dawley rats (weight 330–370 g). After anesthetization (2% isoflurane with oxygen flow of 1.5 L/min) the rats were administrated with the [^{11}C]**13** (30–42 MBq (0.81–1.14 mCi) using tail vein injection and sacrificed by decapitation at the time points 5, 20, 30 or 40 min after administration of the radioactivity. The tissue samples including blood, midbrain, cerebellum, cortex, lung, heart, liver, spleen, kidney and muscle were rapidly collected into pre-weighted gamma-counting tubes and measured with standards (samples of [^{11}C]**13**) using PerkinElmer Wizard2 2480 gamma-counter. Tubes were weighted, and the net mass of the tissue samples was determined and the percent of the injected radioactivity (% ID/g) in the samples was calculated.

In vivo characterization.

Altogether twelve normal Sprague Dawley rats (male, 275–500 g) were used in sixteen studies to investigate *in vivo* imaging characteristics of [^{11}C]**13**. Four rats had control studies followed by the "blocking" studies while three rats had only "blocking" studies and 5 rats had only control studies to investigate binding characteristics of [^{11}C]**13**. For the imaging studies rats were anesthetized with isoflurane/nitrous oxide (1.0–1.5% isoflurane, with oxygen flow of 1–1.5 L/min) and the tail vein was catheterized for administration of the imaging ligand ([^{11}C]**13**). The rats were adjusted into the scanner for imaging position (Triumph II Preclinical Imaging System, Trifoil Imaging,LLC, Northridge, CA). The vital signs such as heart rate and/or breathing were monitored throughout the imaging. Data

acquisition of 60 min was started from the injection of radioligand [^{11}C]**13** (20–41 MBq (0.54–1.11mCi) i.v.).

The “cold” compounds **13** and **17** were used to investigate selectivityand sensitivity of [^{11}C]**13** for the mGluR2. For injection **13** was dissolved into a saline solution with 10% DMSO, 5% Tween-20 and 85% PBS with a pH of 7.4 and **17** was dissolved into saline with 20% HP-B-CD with pH under 5.5. The “cold” compounds were administered (i.v., 4 mg/kg) 10 min before the radioactivity.

CT scan was performed after every PET imaging study to obtain anatomical information and correction for attenuation. The PET imaging data were corrected for uniformity, scatter, and attenuation and processed by using maximum-likelihood expectation-maximization (MLEM) algorithm with 30 iterations to dynamic volumetric images (18×10”, 14×30”, 20×60”, 10×180”). CT data were reconstructed by the modified Feldkamp algorithm using matrix volumes of 512×512×512 and pixel size of 170 μm. The ROIs, i.e., whole brain, thalamus, hippocampus, cortex, striatum, and cerebellum, were drawn onto coronal PET slices according to the brain outlines as derived from the rat brain atlas and corresponding TACs (time-activity curves) were created by PMOD 3.2 (PMOD Technologies Ltd., Zurich, Switzerland). Percent changes between the control and blocking studies were calculated in the selected brain areas at the 10–30 min time window after injection of [^{11}C]**13**.

Supplementary Material

Refer to Web version on PubMed Central for supplementary material.

ACKNOWLEDGEMENTS

This project was financially supported by NIH grants [1R01EB021708 and 1R01NS100164] and the grants 1S10RR023452–01 and 1S10OD025234–01 for the imaging instrumentation and characterization of the organic compounds. mGluR1–6 and mGluR8 agonist and antagonist functional data as well as mGluR2 PAM activity were generously provided by the National Institute of Mental Health’s Psychoactive Drug Screening Program, Contract # HHSN-271–2013-00017-C (NIMH PDSP). The NIMH PDSP is Directed by Bryan L. Roth (mailto:bryan_roth@med.unc.edu) at the University of North Carolina at Chapel Hill and Project Officer Jamie Driscoll (mailto:jdrisco1@mail.nih.gov) at NIMH, Bethesda MD, USA. For experimental details please refer to the PDSP web site https://pdspdb.unc.edu/pdspWeb/ (https://pdspdb.unc.edu/pdspWeb/).

ABBREVIATIONS USED

BBB	blood-brain barrier
VFTD	Venus flytrap domain
7-TM	seven transmembrane
CRD	cysteine rich domain
POOL	Partial Order Optimum Likelihood
EL2	extracellular loop 2
PDB	Protein Data Bank

PAM	positive allosteric modulator
NAM	negative allosteric modulator
MW	molecular weight
tPSA	topological polar surface area
Cl_{int}	the intrinsic clearance
G_i	adenylate cyclase inhibitory G-protein
MWCO	molecular weight cut off
ND	not determined
PBL	Polar brain lipid
PBL	porcine polar brain lipid
P-gp	P-glycoprotein
PAMPA	parallel artificial membrane permeability assay
P_e	effective permeability
EOS	end of synthesis
SWFI	sterile water for injection
TAC	time-activity curve
SUV	standardized uptake value
USP	United States Pharmacopeia
% ID/g	percentage of injected dose per gram of wet tissue

REFERENCES

(1). Tanabe Y; Masu M; Ishii T; Shigemoto R; Nakanishi S A family of metabotropic glutamate receptors. Neuron 1992, 8, 169–179. [PubMed: 1309649]

(2). Cartmell J; Schoepp DD Regulation of neurotransmitter release by metabotropic glutamate receptors. J. Neurochem 2000, 75, 889–907. [PubMed: 10936169]

(3). Gu G; Lorrain DS; Wei H; Cole RL; Zhang X; Daggett LP; Schaffhauser HJ; Bristow LJ; Lechner SM Distribution of metabotropic glutamate 2 and 3 receptors in the rat forebrain: Implication in emotional responses and central disinhibition. Brain Res 2008, 1197, 47–62. [PubMed: 18242587]

(4). Wright RA; Johnson BG; Zhang C; Salhoff C; Kingston AE; Calligaro DO; Monn JA; Schoepp DD; Marek GJ CNS distribution of metabotropic glutamate 2 and 3 receptors: transgenic mice and [3H]LY459477 autoradiography. Neuropharmacology 2013, 66, 89–98. [PubMed: 22313530]

(5). Yin S; Noetzel MJ; Johnson KA; Zamorano R; Jalan-Sakrikar N; Gregory KJ; Conn PJ; Niswender CM Selective actions of novel allosteric modulators reveal functional heteromers of metabotropic glutamate receptors in the CNS. J. Neurosci 2014, 34, 79–94. [PubMed: 24381270]

(6). Kim SH; Fraser PE; Westaway D; George-Hyslop PHS; Ehrlich ME; Gandy S Group II metabotropic glutamate receptor stimulation triggers production and release of Alzheimer's

amyloid β42 from isolated intact nerve terminals. J. Neurosci 2010, 30, 3870–3875. [PubMed: 20237257]

(7). Richards G; Messer J; Faull RLM; Stadler H; Wichmann J; Huguenin P; Bohrmann B; Mutel V Altered distribution of mGlu2 receptors in β-amyloid-affected brain regions of Alzheimer cases and aged PS2APP mice. Brain Res 2010, 1363, 180–190. [PubMed: 20875805]

(8). Lee H.-g.; Ogawa O; Zhu X; O'Neill MJ; Petersen RB; Castellani RJ; Ghanbari H; Perry G; Smith MA Aberrant expression of metabotropic glutamate receptor 2 in the vulnerable neurons of Alzheimer's disease. Acta Neuropathol 2004, 107, 365–371. [PubMed: 14872255]

(9). Caraci F; Molinaro G; Battaglia G; Giuffrida ML; Riozzi B; Traficante A; Bruno V; Cannella M; Merlo S; Wang X; Heinz BA; Nisenbaum ES; Britton TC; Drago F; Sortino MA; Copani A; Nicoletti F Targeting group II metabotropic glutamate (mGlu) receptors for the treatment of psychosis associated with Alzheimer's disease: selective activation of mGlu2 receptors amplifies β-amyloid toxicity in cultured neurons, whereas dual activation of mGlu2 and mGlu3 receptors is neuroprotective. Mol. Pharmacol 2011, 79, 618–626. [PubMed: 21159998]

(10). Moreno JL; Sealfon SC; Gonzalez-Maeso J Group II metabotropic glutamate receptors and schizophrenia. Cell. Mol. Life Sci 2009, 66, 3777–3785. [PubMed: 19707855]

(11). Chaki S Group II metabotropic glutamate receptor agonists as a potential drug for schizophrenia. Eur. J. Pharmacol 2010, 639, 59–66. [PubMed: 20371240]

(12). Downing AM; Kinon BJ; Millen BA; Zhang L; Liu L; Morozova MA; Brenner R; Rayle TJ; Nisenbaum L; Zhao F; Gomez JC A double-bind, placebo-controlled comparator study of LY2140023 monohydrate in patients with schizophrenia. BMC Psychiatry 2014, 14, 351. [PubMed: 25539791]

(13). Patil S; Zhang L; Martenyi F; Lowe SL; Jackson KA; Andreev BV; Avedisova AS; Bardenstein LM; Gurovich IY; Morozova MA; Mosolov SN; Neznanov NG; Reznik AM; Smulevich AB; Tochilov VA; Johnson BG; Monn JA; Schoepp DD Activation of mGluR2/3 receptors as a new approach to treat schizophrenia: a randomized Phase 2 clinical trial. Nat. Med 2007, 13, 1102–1107. [PubMed: 17767166]

(14). Feyissa AM; Woolverton WL; Miguel-Hidalgo JJ; Wang Z; Kyle PB; Hasler G; Stockmeier CA; Iyo AH; Karolewicz B Elevated level of metabotropic glutamate receptor 2/3 in the prefrontal cortex in major depression. Prog. Neuro-psychoph 2010, 34, 279–283.

(15). Johnson MP; Barda D; Britton TC; Emkey R; Hornback WJ; Jagdmann GE; McKinzie DL; Nisenbaum ES; Tizzano JP; Schoepp DD Metabotropic glutamate 2 receptor potentiators: receptor modulation, frequency-dependent synaptic activity, and efficacy in preclinical anxiety and psychosis model(s). Psychopharmacology (Berl) 2005, 179, 271–83. [PubMed: 15717213]

(16). Mazzitelli M; Palazzo E; Maione S; Neugebauer V Group II metabotropic glutamate receptors: role in pain mechanisms and pain modulation. Front Mol. Neurosci 2018, 11, 383. [PubMed: 30356691]

(17). Chiechio S; Copani A; Zammataro M; Battaglia G; Gereau RWIV; Nicoletti F Transcriptional regulation of type-2 metabotropic glutamate receptors: an epigenetic path to novel treatments for chronic pain. Trends Pharmacol. Sci 2010, 31, 153–160. [PubMed: 20064669]

(18). Niswender CM; Conn PJ Metabotropic glutamate receptors: physiology, pharmacology, and disease. Annu. Rev. Pharmacol. Toxicol 2010, 50, 295–322. [PubMed: 20055706]

(19). Marek GJ When is a Proof-of-Concept (POC) not a POC? Pomaglumetad (LY2140023) as a Case Study for Antipsychotic Efficacy. Curr. Pharm. Des 2015, 21, 3788–3796. [PubMed: 26044978]

(20). Adams DH; Kinon BJ; Baygani S; Millen BA; Velona I; Kollack-Walker S; Walling DP A long-term, phase 2, multicenter, randomized, open-label, comparative safety study of pomaglumetad methionil (LY2140023 monohydrate) versus atypical antipsychotic standard of care in patients with schizophrenia. BMC Psychiatry 2013, 13, 143. [PubMed: 23694720]

(21). Stauffer VL; Millen BA; Andersen S; Kinon BJ; Lagrandeur L; Lindenmayer JP; Gomez JC Pomaglumetad methionil: no significant difference as an adjunctive treatment for patients with prominent negative symptoms of schizophrenia compared to placebo. Schizophr Res 2013, 150, 434–441. [PubMed: 24035403]

(22). Fell MJ; Svensson KA; Johnson BG; Schoepp DD Evidence for the role of metabotropic glutamate (mGlu)2 not mGlu3 receptors in the preclinical antipsychotic pharmacology of

the mGlu2/3 receptor agonist (−)-(1R,4S,5S,6S)-4-amino-2- sulfonylbicyclo[3.1.0]hexane-4,6-dicarboxylic acid (LY404039). J. Pharmacol. Exp. Ther 2008, 326, 209–217. [PubMed: 18424625]

(23). Woolley ML; Pemberton DJ; Bate S; Corti C; Jones DNC The mGlu2 but not the mGlu3 receptor mediates the actions of the mGluR2/3 agonist, LY379268, in mouse models predictive of antipsychotic activity. Psychopharmacology (Berlin, Germany) 2008, 196, 431–440.

(24). Yu M; Nagren K; Chen YI; Livni E; Elmaleh D; Kozikowski A; Wang X; Jokivarsi K; Brownell A-L Radiolabeling and biodistribution of methyl 2-(methoxycarbonyl)-2-(methylamino) bicyclo [2.1.1]-hexane-5-carboxylate, a potent neuroprotective drug. Life Sci 2003, 73, 1577–1585. [PubMed: 12865097]

(25). Wang J-Q; Zhang Z; Kuruppu D; Brownell A-L Radiosynthesis of PET radiotracer as a prodrug for imaging group II metabotropic glutamate receptors in vivo. Bioorg. Med. Chem. Lett 2012, 22, 1958–1962. [PubMed: 22318160]

(26). Zhang Z; Brownell A-L Imaging of metabotropic glutamate receptors (mGluRs). In Neuroimaging-clinical applications, Bright P, Ed. In Tech-Open Access Publisher: Rijeka, Croatia, 2012; pp 499–532.

(27). Trabanco AA; Cid JM; Lavreysen H; MacDonald GJ; Tresadern G Progress in the development of positive allosteric modulators of the metabotropic glutamate receptor 2. Curr. Med. Chem 2011, 18, 47–68. [PubMed: 21110815]

(28). Sheffler DJ; Pinkerton AB; Dahl R; Markou A; Cosford NDP Recent progress in the synthesis and characterization of group II metabotropic glutamate receptor allosteric modulators. ACS Chem. Neurosci 2011, 2, 382–393. [PubMed: 22860167]

(29). Andres J-I; Alcazar J; Cid JM; De Angelis M; Iturrino L; Langlois X; Lavreysen H; Trabanco AA; Celen S; Bormans G Synthesis, evaluation, and radiolabeling of new potent positive allosteric modulators of the metabotropic glutamate receptor 2 as potential tracers for positron emission tomography imaging. J. Med. Chem 2012, 55, 8685–8699. [PubMed: 22992024]

(30). Leurquin-Sterk G; Van Laere K; Koole M; Celen S; Bormans G; Langlois X; Te Riele P; Schmidt Mark E; Van Hecken A; Verbruggen A; de Hoon J; Alcazar J; Andres J-I What we observe in vivo is not always what we see in vitro: development and validation of 11C-JNJ-42491293, a novel radioligand for mGluR2. J. Nucl. Med 2017, 58, 110–116. [PubMed: 27469358]

(31). Lohith T; McQuade P; Salinas C; Anderson M; Reynders T; Bautmans A; Bormans G; Serdons K; Laere KV; Hostetler E First-in-human PET imaging of mGluR2 receptors. J. Nucl. Med 2016, 57, 213.

(32). McQuade P; Joshi A; Miller P; Zeng Z; Purcell M; Gantert L; Holahan M; Meissner R; Uslaner J; Hostetler E Discovery and preclinical evaluation of an mGluR2-NAM PET radioligand. J. Nucl. Med 2016, 57, 290.

(33). Majo V; Prabhakaran J; Simpson N; Arango V; Mann JJ; Kumar DJ Development of a [18F]-labeled positive allosteric modulator of the metabotropic glutamate receptor 2 (mGluR2) as a potential PET tracer. J. Nucl. Med 2016, 54, 1072.

(34). Ma Y; Kumata K; Yui J; Zhang Y; Yamasaki T; Hatori A; Fujinaga M; Nengaki N; Xie L; Wang H; Zhang M-R Synthesis and evaluation of 1-(cyclopropylmethyl)-4-(4-[11C]methoxyphenyl)-piperidin-1-yl-2-oxo-1,2-dihydropyridine-3-carbonitrile ([11C]CMDC) for PET imaging of metabotropic glutamate receptor 2 in the rat brain. Bioorg. Med. Chem 2017, 25, 1014–1021. [PubMed: 28049619]

(35). Kumata K; Yamasaki T; Hatori A; Zhang Y; Mori W; Fujinaga M; Xie L; Okubo T; Nengaki N; Zhang M-R Synthesis and in vitro evaluation of three novel radiotracers for imaging of metabotropic glutamate receptor subtype 2 in rat brain. Bioorg. Med. Chem. Lett 2017, 27, 3139–3143. [PubMed: 28571823]

(36). Zhang X; Kumata K; Yamasaki T; Cheng R; Hatori A; Ma L; Zhang Y; Xie L; Wang L; Kang HJ; Sheffler DJ; Cosford NDP; Zhang MR; Liang SH Synthesis and preliminary studies of a novel negative allosteric modulator, 7-((2,5-Dioxopyrrolidin-1-yl)methyl)-4-(2-fluoro-4-[11C]methoxyphenyl) quinoline-2-carboxamide, for imaging of metabotropic glutamate receptor 2. ACS Chem. Neurosci 2017, 8, 1937–1948. [PubMed: 28565908]

(37). Kumata K; Hatori A; Yamasaki T; Zhang Y; Mori W; Fujinaga M; Xie L; Nengaki N; Zhang MR Synthesis and evaluation of 4-(2-fluoro-4-[11C]methoxyphenyl)-5-((2-methylpyridin-4-

yl)methoxy)picolinamide for PET imaging of the metabotropic glutamate receptor 2 in the rat brain. Bioorg. Med. Chem 2019, 27, 483–491. [PubMed: 30611634]

(38). Li Z; Krause S; Suzuki M; Sasaki T Radiotracer compounds. WO/2016033190-A1, 2016.

(39). Van Gool MLM; Andres-Gil JI; Alcazar-Vaca MJ; Bormans GMR; Celen SJL; Joost V Radiolabelled mGluR2 PET ligands. WO/2016087489-A1, 2016.

(40). D'Alessandro PL; Corti C; Roth A; Ugolini A; Sava A; Montanari D; Bianchi F; Garland SL; Powney B; Koppe EL; Rocheville M; Osborne G; Perez P; de la Fuente J; De Los Frailes M; Smith PW; Branch C; Nash D; Watson SP The identification of structurally novel, selective, orally bioavailable positive modulators of mGluR2. Bioorg. Med. Chem. Lett 2010, 20, 759–762. [PubMed: 20005096]

(41). Efremov IV; Rogers BN; Duplantier AJ; Zhang L; Zhang Q; Maklad NS Azabenzimidazolyl compounds as potentiators of mGluR2 subtype of glutamate receptor and their preparation, pharmaceutical compositions and use in the treatment of diseases. WO/2008012622, 2008.

(42). Zhang L; Brodney MA; Candler J; Doran AC; Duplantier AJ; Efremov IV; Evrard E; Kraus K; Ganong AH; Haas JA; Hanks AN; Jenza K; Lazzaro JT; Maklad N; McCarthy SA; Qian W; Rogers BN; Rottas MD; Schmidt CJ; Siuciak JA; Tingley FD; Zhang AQ 1-[(1-Methyl-1H-imidazol-2-yl)methyl]-4-phenylpiperidines as mGluR2 Positive Allosteric Modulators for the Treatment of Psychosis. J. Med. Chem 2011, 54, 1724–1739. [PubMed: 21366332]

(43). Zhang L; Rogers BN; Duplantier AJ; McHardy SF; Efremov I; Berke H; Qian W; Zhang AQ; Maklad N; Candler J; Doran AC; Lazzaro JT; Ganong AH 3-(imidazolylmethyl)-3-aza-bicyclo[3.1.0]hexan-6-yl)methyl ethers: a novel series of mGluR2 positive allosteric modulators. Bioorg. Med. Chem. Lett 2008, 18, 5493–5496. [PubMed: 18812259]

(44). Cid JM; Tresadern G; Vega JA; de Lucas AI; del Cerro A; Matesanz E; Linares ML; Garcia A; Iturrino L; Perez-Benito L; Macdonald GJ; Oehlrich D; Lavreysen H; Peeters L; Ceusters M; Ahnaou A; Drinkenburg W; Mackie C; Somers M; Trabanco AA Discovery of 8-trifluoromethyl-3-cyclopropylmethyl-7-[(4-(2,4-difluorophenyl)-1-piperazinyl)methyl]-1,2,4-triazolo[4,3-a]pyridine (JNJ-46356479), a selective and orally bioavailable mGlu2 receptor positive allosteric modulator (PAM). J. Med. Chem 2016, 59, 8495–8507. [PubMed: 27579727]

(45). Krieger E; Joo K; Lee J; Lee J; Raman S; Thompson J; Tyka M; Baker D; Karplus K Improving physical realism, stereochemistry, and side-chain accuracy in homology modeling: Four approaches that performed well in CASP8. Proteins 2009, 77, 114–122. [PubMed: 19768677]

(46). McGuffin LJ; Shuid AN; Kempster R; Maghrabi AHA; Nealon JO; Salehe BR; Atkins JD; Roche DB Accurate template-based modeling in CASP12 using the IntFOLD4-TS, ModFOLD6, and ReFOLD methods. Proteins 2018, 86, 335–344. [PubMed: 28748648]

(47). Waterhouse A; Bertoni M; Bienert S; Studer G; Tauriello G; Gumienny R; Heer FT; de Beer TAP; Rempfer C; Bordoli L; Lepore R; Schwede T SWISS-MODEL: homology modelling of protein structures and complexes. Nucleic Acids Res 2018, 46, W296–W303. [PubMed: 29788355]

(48). Eisenberg D; Luthy R; Bowie JU VERIFY3D: assessment of protein models with three-dimensional profiles. Methods Enzymol 1997, 277, 396–404. [PubMed: 9379925]

(49). Colovos C; Yeates TO Verification of protein structures: patterns of nonbonded atomic interactions. Protein Sci 1993, 2, 1511–1519. [PubMed: 8401235]

(50). Tong WX; Wei Y; Murga LF; Ondrechen MJ; Williams RJ Partial Order Optimum Likelihood (POOL): Maximum likelihood prediction of protein active site residues using 3D structure and sequence properties. PLoS Comput. Biol 2009, 5, 1–15.

(51). Tan KP; Varadarajan R; Madhusudhan MS DEPTH: a web server to compute depth and predict small-molecule binding cavities in proteins. Nucleic Acids Res 2011, 39, W242–W248. [PubMed: 21576233]

(52). Huang BD MetaPocket: A meta spproach to improve protein ligand binding site prediction. OMICS 2009, 13, 325–330. [PubMed: 19645590]

(53). Morris GM; Goodsell DS; Halliday RS; Huey R; Hart WE; Belew RK; Olson AJ Automated docking using a Lamarckian genetic algorithm and an empirical binding free energy function. J. Comput. Chem 1998, 19, 1639–1662.

(54). Perez-Benito L; Doornbos MLJ; Cordomi A; Peeters L; Lavreysen H; Pardo L; Tresadern G Molecular switches of allosteric modulation of the metabotropic glutamate 2 receptor. Structure 2017, 25, 1153–1162. [PubMed: 28648611]

(55). Doornbos MLJ; Cid JM; Haubrich J; Nunes A; van de Sande JW; Vermond SC; Mulder-Krieger T; Trabanco AA; Ahnaou A; Drinkenburg WH; Lavreysen H; Heitman LH; AP IJ; Tresadern G Discovery and kinetic profiling of 7-aryl-1,2,4-triazolo[4,3-a]pyridines: positive allostericmodulators of the metabotropic glutamate receptor 2. J. Med. Chem 2017, 60, 6704–6720. [PubMed: 28704052]

(56). Doornbos ML; Perez-Benito L; Tresadern G; Mulder-Krieger T; Biesmans I; Trabanco AA; Cid JM; Lavreysen H; AP IJ; Heitman LH Molecular mechanism of positive allosteric modulation of the metabotropic glutamate receptor 2 by JNJ-46281222. Br. J. Pharmacol 2016, 173, 588–600. [PubMed: 26589404]

(57). Poutiainen P; Kil KE; Zhang Z; Kuruppu D; Tannous B; Brownell A-L Co-operative binding assay for the characterization of mGlu4 allosteric modulators. Neuropharmacology 2015, 97, 142–148. [PubMed: 26025660]

(58). Kil KE; Poutiainen P; Zhang Z; Zhu A; Choi JK; Jokivarsi K; Brownell A-L Radiosynthesis and evaluation of an 18F-labeled positron emission tomography (PET) radioligand for metabotropic glutamate receptor subtype 4 (mGlu4). J. Med. Chem 2014, 57, 9130–9138. [PubMed: 25330258]

(59). Roth BL Assay protocol book. In Version III ed.; PDSP, N., Ed. Department of Pharmacology, University of North Carolina at Chapel Hill, 2018.

(60). DiRaddo JO; Miller EJ; Hathaway HA; Grajkowska E; Wroblewska B; Wolfe BB; Liotta DC; Wroblewski JT A real-time method for measuring cAMP production modulated by Gαi/o-coupled metabotropic glutamate receptors. J. Pharmacol. Exp. Ther 2014, 349, 373–382. [PubMed: 24659805]

(61). Jin X; Semenova S; Yang L; Ardecky R; Sheffler DJ; Dahl R; Conn PJ; Cosford NDP; Markou A The mGluR2 positive allosteric modulator BINA decreases cocaine self-administration and cue-induced cocaine-seeking and counteracts cocaine-induced enhancement of brain reward function in rats. Neuropsychopharmacol 2010, 35, 2021–2036.

(62). Minick DJ; Frenz JH; Patrick MA; Brent DA A comprehensive method for determining hydrophobicity constants by reversed-phase high-performance liquid chromatography. J. Med. Chem 1988, 31, 1923–1933. [PubMed: 3172126]

(63). Pike VW PET radiotracers: crossing the blood-brain barrier and surviving metabolism. Trends Pharmacol. Sci 2009, 30, 431–440. [PubMed: 19616318]

(64). Banker MJ; Clark TH; Williams JA Development and validation of a 96-well equilibrium dialysis apparatus for measuring plasma protein binding. J. Pharm. Sci 2003, 92, 967–974. [PubMed: 12712416]

(65). Di L; Kerns EH; Hong Y; Chen H Development and application of high throughput plasma stability assay for drug discovery. Int. J. of Pharm 2005, 297, 110–119. [PubMed: 15876500]

(66). Houston JB Utility of in vitro drug metabolism data in predicting in vivo metabolic clearance. Biochem. Pharmacol 1994, 47, 1469–79. [PubMed: 8185657]

(67). Engers DW; Niswender CM; Weaver CD; Jadhav S; Menon UN; Zamorano R; Conn PJ; Lindsley CW; Hopkins CR Synthesis and evaluation of a series of heterobiarylamides that are centrally penetrant metabotropic glutamate receptor 4 (mGluR4) positive allosteric modulators (PAMs). J. Med. Chem 2009, 52, 4115–4118. [PubMed: 19469556]

(68). Kil K-E; Zhang Z; Jokivarsi K; Gong C; Choi J-K; Kura S; Brownell A-L Radiosynthesis of N-(4-chloro-3-[11C]methoxyphenyl)-2-picolinamide ([11C]ML128) as a PET radiotracer for metabotropic glutamate receptor subtype 4 (mGlu4). Bioorg. Med. Chem 2013, 21, 5955–5962. [PubMed: 23978356]

(69). Di L; Kerns EH; Chen H; Petusky SL Development and application of an automated solution stability assay for drug discovery. J. Biomol. Screen 2006, 11, 40–47. [PubMed: 16234336]

(70). Di L; Kerns EH; Fan K; McConnell OJ; Carter GT High throughput artificial membrane permeability assay for blood-brain barrier. Eur. J. Med. Chem 2003, 38, 223–232. [PubMed: 12667689]

(71). Promega. Pgp-Glo Assay System, Instructions for use of products V3591 and V3601. In Technical bulletin, Promega: 2015.

(72). Altschul SF; Madden TL; Schaffer AA; Zhang JH; Zhang Z; Miller W; Lipman DJ Gapped BLAST and PSI-BLAST: a new generation of protein database search programs. Nucleic Acids Res 1997, 25, 3389–3402. [PubMed: 9254694]

(73). Kunishima N; Shimada Y; Tsuji Y; Sato T; Yamamoto M; Kumasaka T; Nakanishi S; Jingami H; Morikawa K Structural basis of glutamate recognition by a dimeric metabotropic glutamate receptor. Nature 2000, 407, 971–977. [PubMed: 11069170]

(74). Dobrovetsky E; Khutoreskaya G; Seitova A; Cossar D; Edwards AM; Arrowsmith CH; Bountra C; Weigelt J; Bochkarev A Ligand binding domain of metabotropoc glutamate receptor mGluR5 complexed with glutamate RCSB Protein Data Bank, 2017, DOI:10.2210/pdb3LMK/pdb

(75). Koehl A; Hu HL; Feng D; Sun BF; Zhang Y; Robertson MJ; Chu M; Kobilka TS; Laermans T; Steyaert J; Tarrasch J; Dutta S; Fonseca R; Weis WI; Mathiesen JM; Skiniotis G; Kobilka BK Structural insights into the activation of metabotropic glutamate receptors. Nature 2019, 566, 79–84. [PubMed: 30675062]

(76). Hanwell MD; Curtis DE; Lonie DC; Vandermeersch T; Zurek E; Hutchison GR Avogadro: an advanced semantic chemical editor, visualization, and analysis platform. J. Cheminformatics 2012, 4, 1–17.

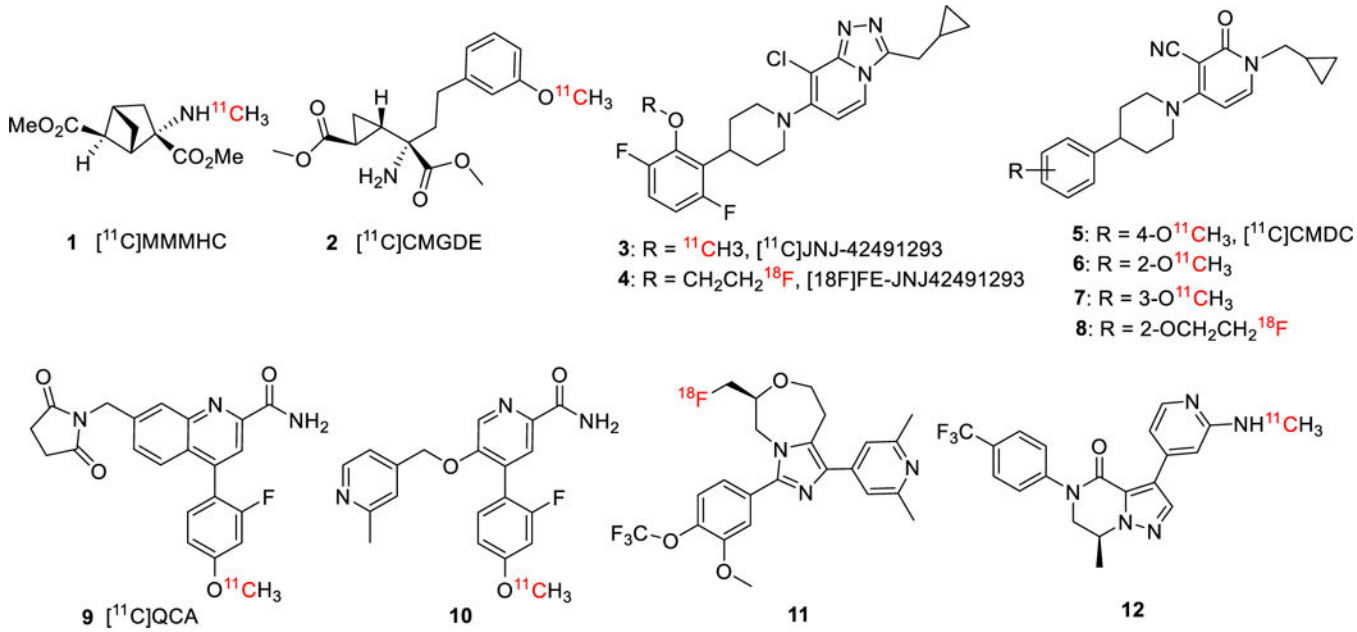

Figure 1.
Typical PET radiotracers for mGluR2.

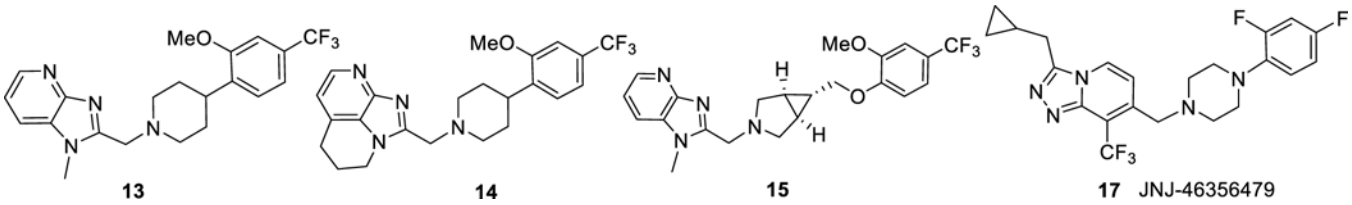

Figure 2.
Chemical structures of compounds **13**-**15** and **17**.

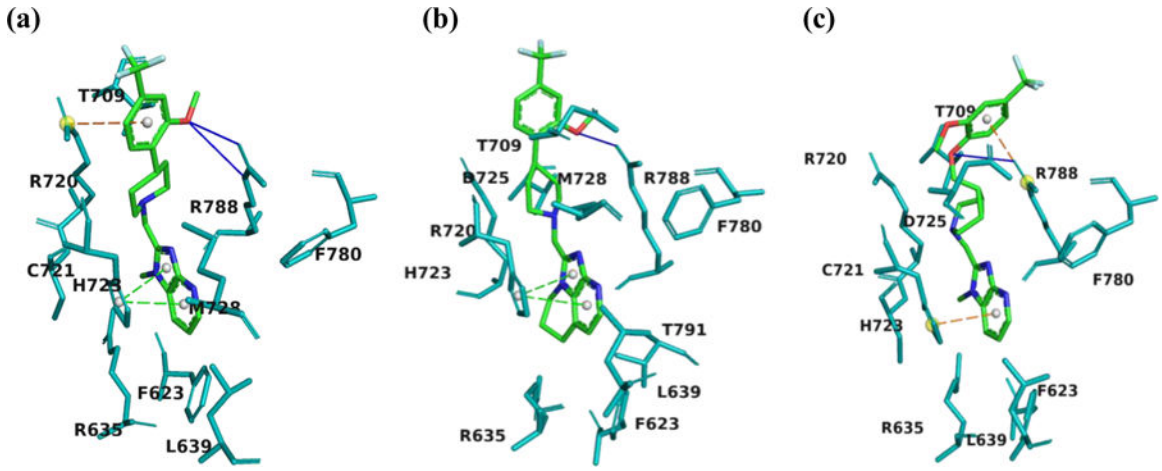

Figure 3.

Snapshots of the docking results for compounds **13** (**a**), **14** (**b**) and **15** (**c**). Pictures were rendered in PyMol 2.3.3. The interacting residues are shown in teal. The ligand atoms are rendered as carbon in green, nitrogen in blue, oxygen in red, and fluorine in cyan. Blue lines represent H-bonds, green dotted lines show π-π stacking, and orange dotted lines indicate π-cation interaction.

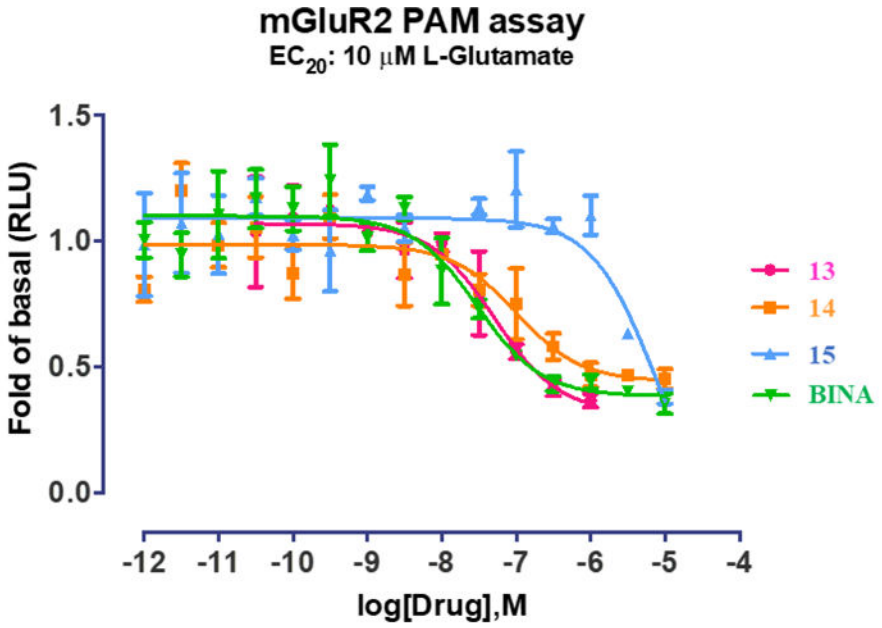

Compound	13	14	15	BINA
EC_{50}	5.12E-08	1.01E-07	7.81E-06	2.97E-08

Figure 4.
The mGluR2 PAM activity.

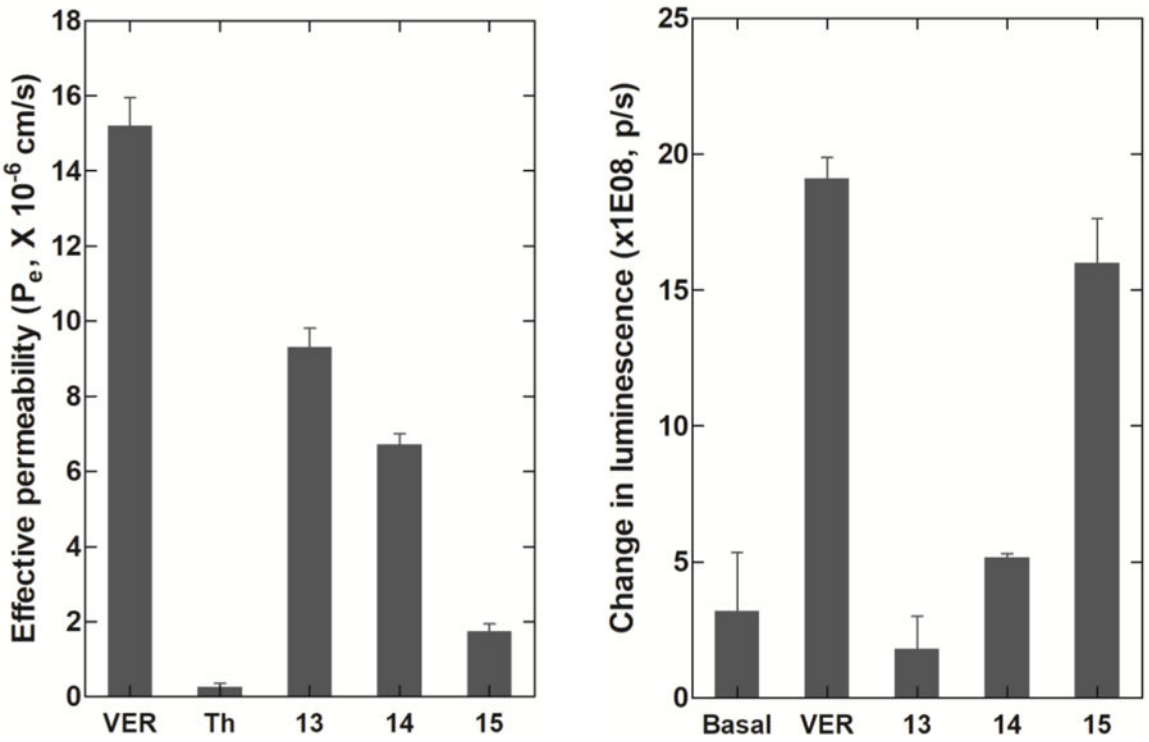

Figure 5.

Assessment of BBB permeability for compounds **13–15** via **a**) PAMPA assay and **b**) Pgp-Glo™ assay. Pictures were rendered from Prism 5.0.

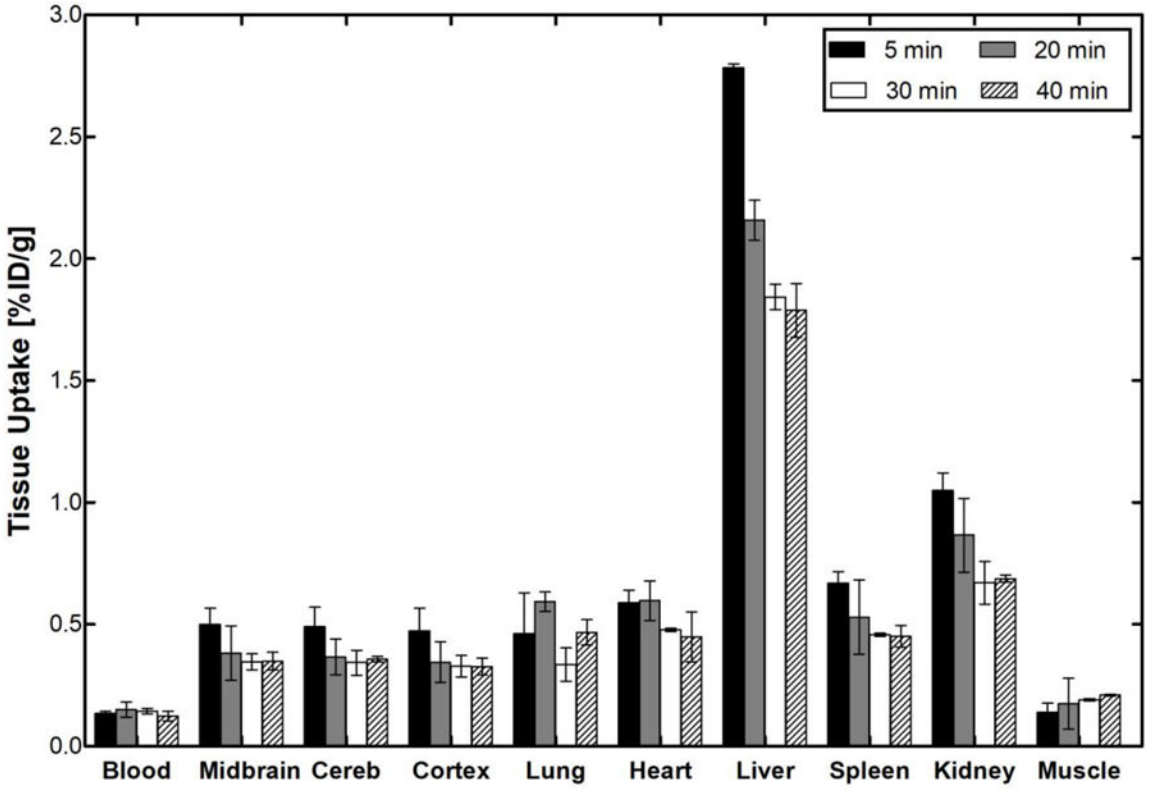

Figure 6.

The *ex vivo* biodistribution in rat at four different time points post-[^{11}C]**13** injection. Picture was rendered from Prism 5.0.

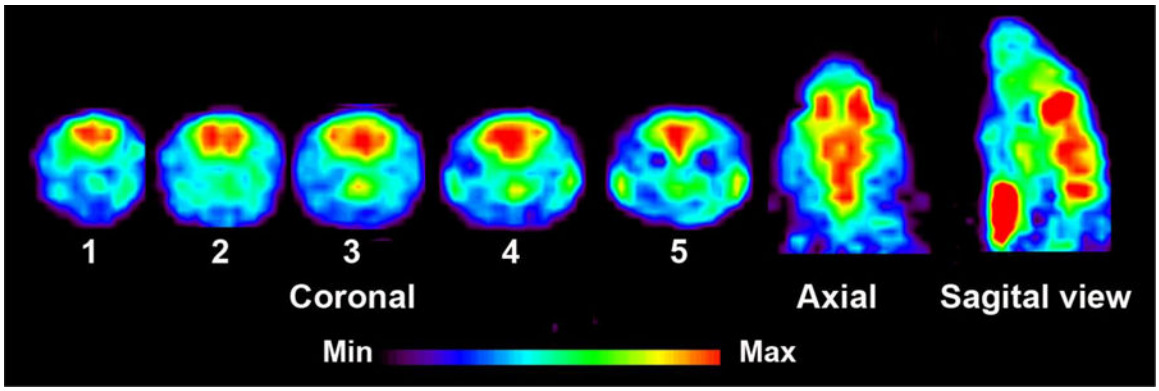

Figure 7.

PET images of [^{11}C]**13** uptake in the rat brain at the time interval 10–15 min. Coronal level 1 shows uptake in the cingulate and motor cortex; level 2 in the striatum, level 3 in the thalamus and striatum, level 4 in the thalamus and hippocampus and level 5 in the cerebellum. Axial and sagittal views show activity distribution in the midbain level. Slice thickness is 1.25 mm.

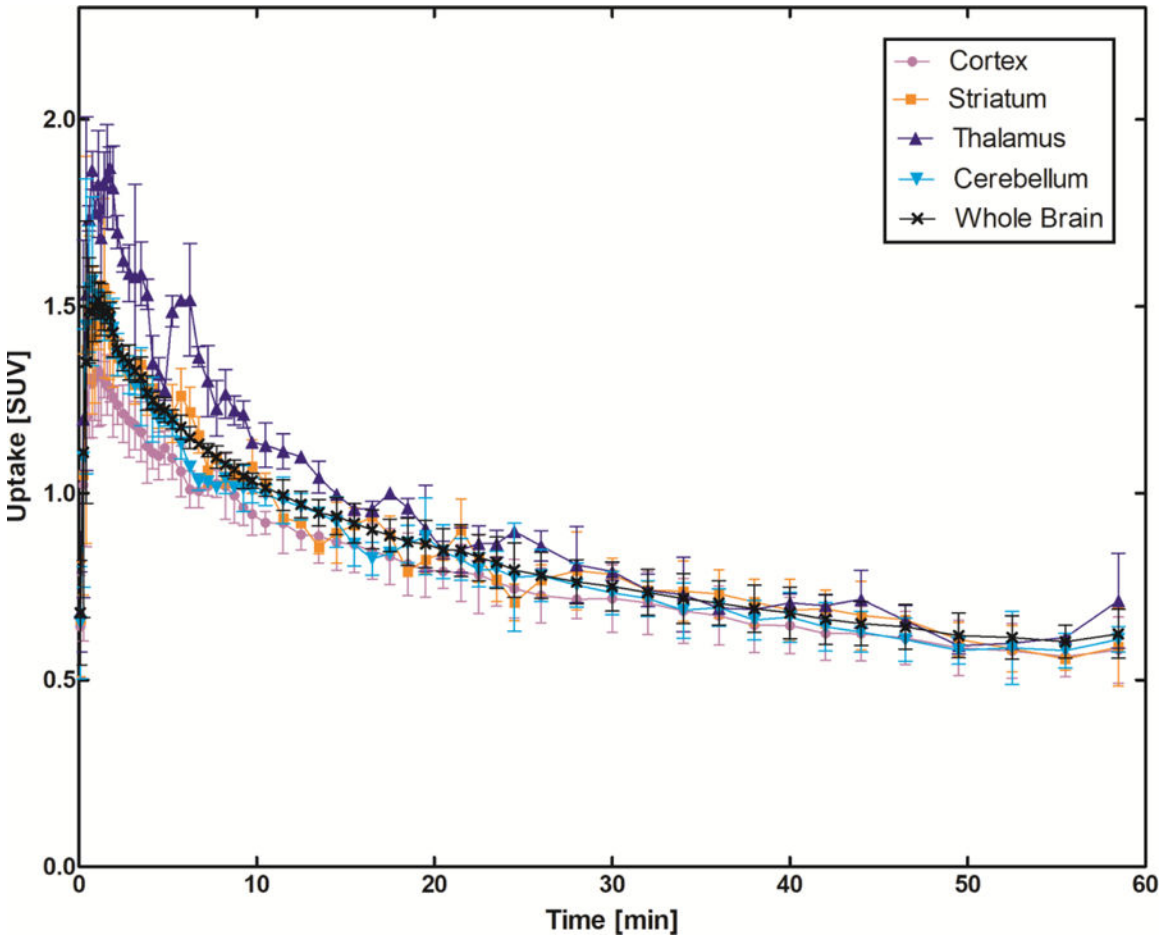

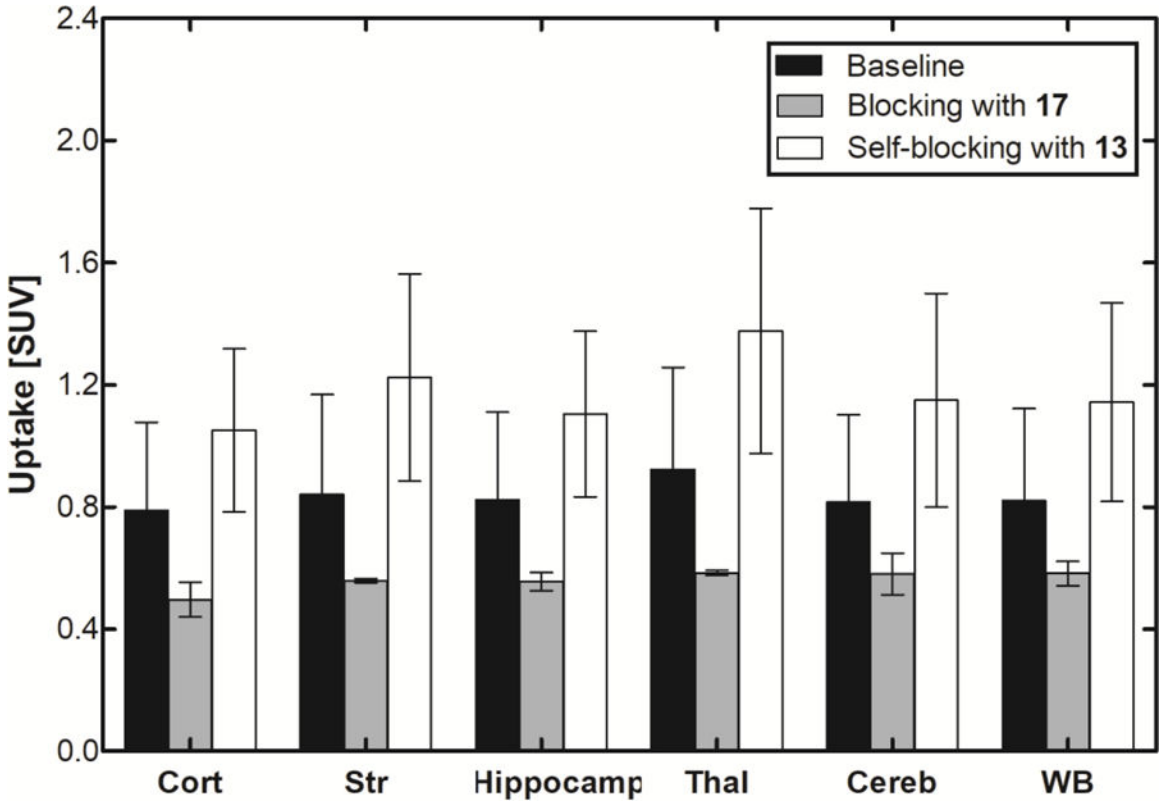

Figure 8.

In vivo binding profile of [^{11}C]**13** in the rat brain. **a**) Time–activity distribution of [^{11}C]**13** in different brain areas show fast accumulation and reversible binding. The data is averaged of six normal Sprague Dawley rats. **b**) The blocking effect was calculated in the time interval 10–30 min after administration of [^{11}C]**13**. Cort = cortex, Str = striatum, Hippocamp = hippocampus, Thal = thalamus, Cereb = cerebellum and WB = whole brain. Pictures were rendered from Prism 5.0.

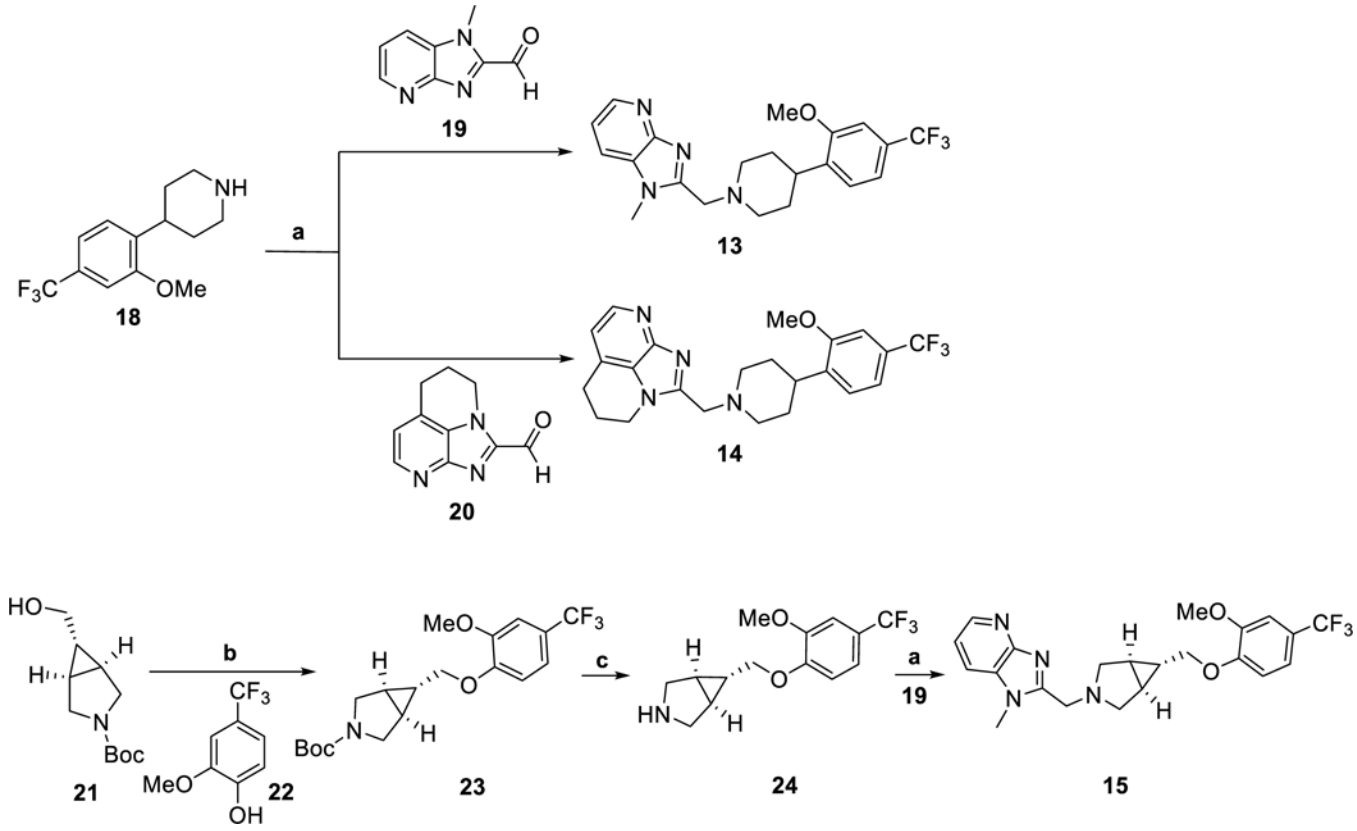

Scheme 1.

Syntheses of **13–15.** Reagents and conditions: (a) Et3N, MgSO4, then Na(OAc)3BH, DCE, rt, overnight; (b) PPh3, diethyl azodicarboxylate solution (40 wt.% in toluene), THF, rt, 16 h; (c) TFA, DCM, rt, 2 h.

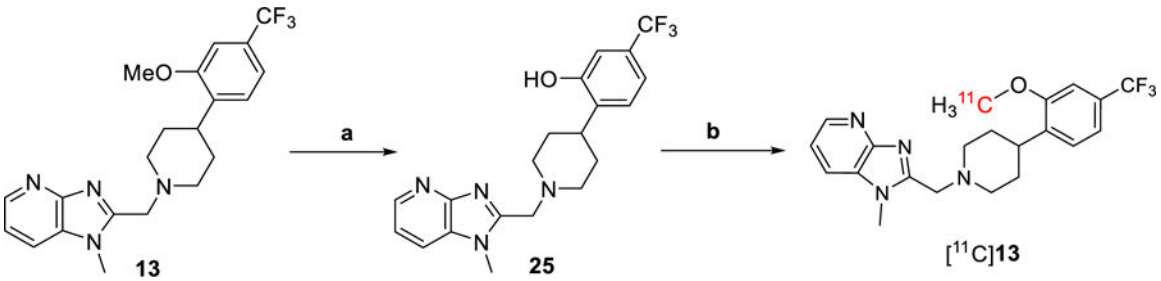

Scheme 2.

Synthesis of [$_{11}$C]**13**. Reagents and conditions: (a) BBr_3, DCM, 0 ℃ then rt, 2 h. (b) [^{11}C]CH_3I, 5N NaOH, DMF, rt, then 80 ℃, 2 min.

Table 1.

Binding affinity of compounds **13**-**15** to mGluR2.

Compound	13	14	15
IC_{50} ± SEM (nM)	7.6 ± 0.9	10.5 ± 0.5	10.5 ± 7.9
log (IC_{50} ± SEM)	−8.12 ± 0.79	−7.98 ± 0.21	−7.98 ± 1.39

Table 2.

Physicochemical properties of compounds **13-15**

Compound	MW (g/mol)	tPSA	HBD	cLogP	Log P	PPB ± SEM (%)
13	404.44	40.43	1	3.57	3.65	87.2 ± 0.1
14	430.48	40.43	1	4.08	3.86	88.7 ± 0.1
15	432.45	49.66	1	2.89	3.3	---

Table 3.

The *in vitro* stability of compounds **13-15**

Compound	The plasma stability	The microsome stability		The solution stability		
	The intact ± SEM at 120 min (%)	$t_{1/2}$ (min)	CL_{int} (mL/min/mg protein)	The intact ± SEM at 120 min (%)		
				pH = 5.0	pH = 7.4	pH = 9.4
13	96.6 ± 2.1	74.5	17.9	95.3 ± 0.3	94.5 ± 0.4	96.1 ± 0.7
14	89.2 ± 0.6	73.7	18.1	---	---	---
Diltiazem	43.2 ± 0.8	---	---	---	---	---
ML128	---	4.2	317.1	---	---	---